Algal CO_2 capture is powered by alternative electron pathways of photosynthesis

Authors: Gilles Peltier[1], Carolyne Stoffel[2], Justin Findinier[2], Sai Kiran Madireddi[2], Ousmane Dao[1], Virginie Epting[1], Arthur Grossman[2,3], Yonghua Li-Beisson[1], Adrien Burlacot[2,3*]

Affiliations:

[1] Aix Marseille Univ, CEA, CNRS, Institut de Biosciences et Biotechnologies Aix-Marseille, CEA Cadarache, 13108 Saint Paul-lez-Durance, France

[2] Department of Plant Biology, The Carnegie Institution for Science, Stanford, CA, 94305 USA

[3] Department of Biology, Stanford University, Stanford, CA, 94305, USA

[*]corresponding author: A.B., aburlacot@carnegiescience.edu

ORCID IDs: 0000-0001-7434-6416 (A.B.), 0000-0002-4078-6250 (C.S.), 0000-0001-9019-8900 (J.F.), 0000-0002-1820-1033 (S.M.), 0000-0002-7040-5770 (O.D), 0000-0003-1064-1816 (Y.L.-B.), 0000-0002-3747-5881(A.G.), 0000-0002-2226-3931 (G.P.)

Author contributions: A.B. led and coordinated the research, A.B. and G.P. designed research; A.B., C.S., J.F., O.D., S.M., V.E. and G.P. performed research; A.B. and G.P. contributed new reagents/analytic tools; A.B. analyzed data and made all figures; A.B. and G.P. wrote the paper with inputs from Y. L.-B. and A.G.

One sentence summary: Quantifying the contribution of the main electron flow pathways to algal CO_2 fixation.

Abstract

On Earth, microalgae contribute to about half of global net photosynthesis. During photosynthesis, sunlight is converted into chemical energy (ATP and NADPH) used by metabolism to convert CO_2 into biomass. Alternative electron pathways of photosynthesis have been proposed to generate additional ATP that is required for sustaining CO_2 fixation, but the relative importance of each pathway remains elusive. Here, we dissect and quantify the contribution of cyclic, pseudo-cyclic and chloroplast to mitochondria electron flows for their ability to sustain net photosynthesis in the microalga *Chlamydomonas reinhardtii*. We show that each pathway has the potential to energize substantial CO_2 fixation, can compensate each other, and that the additional energy requirement to fix CO_2 is more than 3 times higher than previous estimations. We further show that all pathways have very different efficiencies at energizing CO_2 fixation, with the chloroplast- mitochondria interaction being the most efficient, thus laying bioenergetic foundations for biotechnological improvement of CO_2 capture.

Introduction

Oxygenic photosynthesis is the main process responsible for the carbon input into ecosystems on Earth, with net CO_2 fixation by photosynthesis representing more than ten times anthropic CO_2 emissions [1]. During photosynthesis, carbon fixation is powered by the combined action of photosystems (PS) I and II, establishing a linear electron flow (LEF) that produces reducing power (NADPH) and a trans-thylakoidal proton motive force (*pmf*) used to generate ATP. Both ATP and NADPH fuel the CO_2 fixation reactions of the Calvin-Benson-Bassham (CBB) cycle and the further processing of the glyceraldehyde-3-phosphate (G3P) to regenerated ribulose-1-5 bisphosphate and produce building blocks used for the elaboration of biomass [2]. However, given the insufficiency of the LEF to generate an adequate *pmf* and the conversion efficiency of the chloroplastic ATP-synthase (ATPase), it has been long recognized that the LEF only generates 85% of the theoretical ATP requirements of the CBB cycle [3].

Cyclic electron flow, which recycles reducing equivalents around PSI (CEF) and pseudo-cyclic electron flow (PCEF), which reduces molecular O_2 at the acceptor side of PSI (**Fig. 1**), were proposed to contribute to the production of extra ATP during photosynthesis [4,5]. In most angiosperms and mosses, CEF entails two main pathways, one involving the proton gradient generation (PGR) 5 [6] and PGR-Like 1 proteins [7] and another involving the plastidial NDH-1 complex [8,9]. In green microalgae, the plastidial NDH-1 complex is absent [10] and it was reported that two CEF pathways operate, one controlled by PGRL1 and PGR5 [11,12] and the other involving the plastidial NAD(P)H dehydrogenase Nda2 [13-15], which is mostly active during nitrogen deprivation [15,16]. PCEF involves Flavodiiron proteins (FLVs) that catalyse O_2 photoreduction at the PSI acceptor side (**Fig. 1**) in cyanobacteria [17,18], green microalgae [19], mosses [20], liverwort [21] and gymnosperms [22].

Another mechanism that can supply ATP to photosynthesis involves metabolic cooperation between chloroplasts and mitochondria [23]. Reducing power generated within the chloroplast is transferred to the mitochondria by metabolic shuttles where it is converted into ATP by the mitochondrial respiratory chain and might be shuttled back to the cytosol and the chloroplast (**Fig. 1**). Such a cooperation, called here Chloroplast to Mitochondria Electron Flow (CMEF) was first evidenced from the restoration of photoautotrophic growth in a mutant of the green microalgae *Chlamydomonas reinhardtii* (hereafter *Chlamydomonas*) deficient in the plastidial ATPase [24]. Similar cooperation was later reported in a PGRL1-deficient *Chlamydomonas* mutant [25] and in diatoms [26].

It is generally considered that both PCEF and CMEF act essentially as electron valves, operating either transiently in the case of PCEF to alleviate excess electrons generated by photosynthesis under light fluctuating regimes [19,27,28] or more continuously for CMEF under high light stress [29]. Although in *Chlamydomonas*, CMEF, PCEF and CEF have been recently shown to all contribute to supply energy to the CO_2 concentrating mechanism (CCM) [30], evidence of their role in powering the CBB cycle and downstream carbon metabolism processes are scarce.

In this work, we show that each pathway (CEF, PCEF and CMEF) has the capacity to sustain net CO_2 fixation to varying degrees and can compensate for the absence of the other pathways, whereas CO_2 fixation is completely abolished in the absence of all three pathways. Moreover, we compare the electron quantum yield of net photosynthesis for each pathway and show that CMEF is by far the most efficient at energizing CO_2 fixation. We further discuss our data in relation to the relative contribution and efficiency of the different alternative pathways to the net primary productivity of terrestrial and oceanic ecosystems.

87 **Results**

88 **Net photosynthesis fully relies on mitochondrial respiration when PCEF and CEF are**
89 **impaired.** To test whether PCEF and CEF are required for maximal net photosynthesis (V_{Max}),
90 we first measured photosynthetic O_2 exchange rates using Membrane Inlet Mass Spectrometry
91 [31] in air-grown *Chlamydomonas* mutants impaired in both CEF and PCEF (*pgrl1 flvB-1 and 3*)
92 and in control strains (WT2 and 3)[30]. Since the *pgrl1* and *flvB* mutants are affected in the
93 functioning of the CO_2 concentration mechanism (CCM) [30], photosynthesis measurements were
94 performed in the presence of a saturating concentration of inorganic carbon (C_i) when the CCM
95 is inactive. As previously reported [30], *pgrl1 flvB* double mutants can perform photosynthesis at
96 maximum rates comparable to the single *pgrl1* or *flvB* mutants and to the parental and sibling
97 control strains (**Fig. 2; Sup Figs. S1 A, S2, S3**), therefore showing that neither CEF nor PCEF
98 are essential to reach V_{Max}. To test a possible contribution of mitochondrial respiration to
99 photosynthesis, *pgrl1 flvB* double mutants were treated with myxothiazol (Myxo) and
100 salicylhydroxamic acid (SHAM), inhibitors of mitochondrial electron transport, respectively
101 acting on complex III and the alternative oxidases (AOX) (**Fig. 1**)[32]. While the addition of both
102 inhibitors had minimal impact (about 10-20% decrease) on the V_{Max} of control strains (**Fig. 2**
103 **A, C, Sup Figs. S1 A, S2, S3**), they completely abolished photosynthesis of *pgrl1 flvB* double
104 mutants (**Fig. 2 B, C, Sup Figs. S1, S2)**.

105 In *Chlamydomonas*, the cellular location of mitochondria depends on the CO_2 supply,
106 with the mitochondria located at the cell periphery in low CO_2-grown cells and mostly inside
107 the chloroplast cup in high CO_2 [33] (**Fig. 2E, F**). Since this location might affect the CMEF [34],
108 we sought to examine the involvement of the mitochondrial sub-cellular localization on the role
109 of CMEF. Similar to air-grown cells, mitochondrial inhibitors fully stopped net photosynthesis
110 on 2% CO_2-grown *pgrl1 flvB* mutants while having a marginal effect (about 10-20% decrease)
111 on the control strains (**Fig. 2D, Sup Fig. S4**). To control the location of the mitochondria in the
112 different strains, we visualized the spatial distribution of an expressed, mitochondria-targeted
113 fluorophore (Clover). There was similar re-localization of mitochondria depending on the CO_2
114 supply during growth (at periphery under very low CO_2) of both the single and double mutants
115 and a control strain (**Fig. 2E, F, Sup Fig. S5**). We conclude from this experiment that in the
116 absence of both CEF and PCEF, near wild type levels of photosynthesis can be achieved that
117 fully rely on CMEF, the role of CMEF being independent of the spatial distribution of the
118 mitochondria.

119

120 **CEF, PCEF and CMEF each have the potential to sustain most net photosynthesis.** We
121 quantified the potential of CEF, PCEF and CMEF to energize net photosynthesis, by measuring
122 the effect of mitochondrial inhibitors on photosynthesis rates in single and double *pgrl1* and
123 *flvB* mutants (**Fig. 3 A, B, C, D**). Inhibition of respiration decreased net photosynthesis by 40-
124 50% in both the *flvB* and *pgrl1* single mutants (**Fig. 3 A, B, Sup Figs. S1 A, S2**), showing that
125 both CEF and PCEF have the potential to energize 50-60% of V_{Max} on their own (**Fig. 3 E, Sup**
126 **Fig. S1A, B**). Inhibition of respiration decreased the V_{Max} of all control strains by 10-20% (**Fig.**
127 **S1 A, S2, S3**) showing that combined activities of CEF and PCEF can power approximately
128 85% of photosynthesis (**Fig. 3 E**). Based on the effects of SHAM or myxothiazol individually,
129 on V_{Max} in *pgrl1 flvB* mutants (**Fig. 3C, D, E, Sup Figs. S1 A, S2**), we conclude that while the
130 complex III-IV pathway of CMEF (**Fig. 1**) can power most net photosynthesis on its own (**Fig.**
131 **3D**), the AOX pathway (**Fig. 1**) can only sustain approximately 45% of V_{Max} (**Fig. 3E**). Because
132 the amount of the terminal oxidases involved in CMEF does not differ in the *pgrl1 flvB* mutants
133 and their control strains (**Sup Fig. S6**), these values likely reflect wild type capacities. We also
134 quantified net photosynthesis based on inorganic carbon (C_i) uptake (**Sup Figs. S7, S8**). On all
135 strains tested, the inhibitory effects on V_{max} measured as net C_i uptake was similar to that
136 observed on net O_2 production (**Sup Figs. S7**). We conclude from these experiments that CEF,
137 PCEF and CMEF can sustain photosynthetic C_i uptake on their own but that only the complex
138 III-IV pathway of CMEF is efficient enough to reach near maximal photosynthesis levels.
139
140 **CEF, PCEF and CMEF show different efficiencies in sustaining net photosynthesis.**
141 Mechanistically, for each electron flowing through the different pathways (CEF, PCEF, the
142 AOX, or the complex III-IV pathway of CMEF), the total number of protons translocated across
143 the thylakoid and/or the inner mitochondrial membranes, highly differ (**Table 1**). To quantify
144 the potential of the different pathways in energizing net photosynthesis, we defined the electron
145 (e^-) quantum yield of a pathway by the following equation:

146 $$e^- quantum\ yield = \frac{e^-(net\ photosynthesis)}{e^-(net\ photosynthesis) + e^-(alternative\ pathway)}$$

147 Where e^- (net photosynthesis) is the flux of photosynthetic electrons directly used for net
148 photosynthesis and e^- (alternative pathway) is the flux of photosynthetic electrons through a
149 given alternative pathway under conditions where it is the only alternative pathway active. The
150 e^- quantum yield of an alternative pathway therefore represents the proportion of photosynthetic
151 electrons used in the metabolic reactions of CO_2 assimilation if only this alternative pathway is
152 active. We used this equation and experiments from **Fig. 3 A-E** to quantify the e^- quantum yield

153 of each pathway (**Fig. 3 F, Sup Fig. S9**). The e^-quantum yield of PCEF was estimated at 0.65,
154 whereas that of CMEF at 0.85 (**Fig. 3F**), indicating a better efficiency of CMEF in driving CO_2
155 fixation as compared to PCEF. In the absence of an established method to quantifying CEF in
156 physiologically relevant conditions [30], CEF quantum efficiency was estimated to be around 0.55
157 by hypothesizing that electrons passing through CEF are 1.5 time less efficient at generating a
158 *pmf* than when they pass through PCEF [35] (**see Materials and Methods**). In the case of CMEF,
159 the e^- quantum yield of the AOX pathway was lower than that of the complex III-IV pathway
160 (**Fig. 3F**), likely reflecting the proton translocating capacity of each pathway (**Fig. 1, Table 1**).
161 Using the e^- quantum yields of each pathway, we then compared the flux of electrons required
162 to power the same amount of net photosynthesis relative to PCEF (**Fig. 3G**). Strikingly,
163 theoretical values were in accord with values experimentally determined by the e^- quantum
164 yields (**Fig. 3 G**). We conclude from these experiments that CMEF pathways are more efficient
165 than PCEF and CEF at energizing CO_2 fixation and that this difference arises from a higher
166 H^+/e^- transfer capacity likely leading to a higher capacity to generate ATP.
167
168 **Estimating the respective contributions of CEF, PCEF and CMEF during steady state**
169 **photosynthesis and growth.** We then sought to estimate (*i*) the electron flux via each pathway
170 expressed as an additional electron flow relative to net photosynthesis (*%-LEF*) and (*ii*) their
171 contribution to energize net photosynthesis. Since the electron flux through a given pathway
172 may be affected by the removal of other pathways, we used two different approaches to reach
173 a realistic estimate of electron fluxes, one based on the effect of mutations, and one based on
174 the effect of respiratory inhibitors. In the first approach, PCEF was quantified by subtracting
175 O_2 uptake rates in the *flvB* mutant from its control parental strain (allowing the calculation of
176 $PCEF_{mut}$ and $CMEF_{mut}$) (**Sup Fig. S10**). In the second approach, CMEF was quantified by
177 subtracting O_2 uptake rates between SHAM plus Myxo treated and untreated control strains
178 (allowing the calculation of $PCEF_{inhib}$ and $CMEF_{inhib}$) (**Sup Fig. S10**). The two methods differ
179 somewhat in their estimates of PCEF and CMEF (**Fig. 4 A, B, Sup Fig. S11**), with a higher
180 CMEF contribution being estimated using the mutant method. On average, PCEF and CMEF
181 represent a flux of between 10-20*%-LEF* and 5-10*%-LEF*, respectively (**Fig. 4 A**). Using the e^-
182 quantum yield of each pathway we estimate that 10-30% and 30-60% of CO_2 fixation is
183 sustained by PCEF and CMEF respectively (**Fig. 4 B**). Since CEF sustains the remaining net
184 photosynthesis, we can estimate that 25-30% of CO_2 fixation is powered by CEF (**Fig. 4 B**),
185 which corresponds to a CEF of about 25*%-LEF* (**Fig. 4 A**). Estimations on other control strains
186 using the inhibitor approach show that, while the relative contribution of each pathway varies

187 depending on the strain considered (**Sup Fig. S11**), no single pathway sustains CO_2 fixation by
188 itself (**Sup Fig. S11 B**).
189 To further assess the contribution of CEF, PCEF and CMEF over the long term, growth
190 tests were performed on the different strains in the absence or presence of the respiration
191 inhibitor Myxo. While Myxo has no effect on the growth of control strains and single *flvB* or
192 *pgrl1* mutants in moderate light intensities (**Fig. 4 C**), growth of *pgrl1 flvB* was impaired in the
193 presence of the inhibitor (**Fig. 4 C**). Interestingly, at low light intensity (30 µmol photons m^{-2}
194 s^{-1}), the effect of Myxo on the double mutant was absent (**Sup Fig. 12 A**), suggesting that the
195 AOX pathway of CMEF is sufficient to power net photosynthesis in low light conditions.
196 Therefore, whereas CEF, PCEF, and CMEF all contribute to energizing photosynthesis, CMEF,
197 although representing a relatively small flux, unexpectedly appears to be a major contributor to
198 fuelling CO_2 fixation and biomass accumulation thanks to its high e^- quantum yield.
199
200 **Discussion**
201 Since the first description of CEF by Arnon in 1959 [4], the question was raised as to whether
202 LEF could sustain the ATP requirement of photosynthetic CO_2 fixation [4], and it was proposed
203 that photosynthetic electron flows, other than LEF, are involved in balancing the ATP/NADPH
204 ratio to sustain CCB cycle function [3,4]. Since then, several mechanisms of CEF, PCEF and
205 CMEF have been uncovered [6,8,17,36], but the importance and relative efficiency of each
206 mechanism remain mostly unknown. Here we have shown that in *Chlamydomonas* PGRL1-
207 controlled CEF, FLV-mediated PCEF, and both the AOX and complex III/IV/cytochrome
208 oxidase pathways of CMEF can all supply additional energy to complement LEF for CO_2
209 fixation. The e^- quantum yields of CEF, PCEF and CMEF greatly differ; CMEF is the most
210 electron efficient and contributes importantly to the extra ATP requirements of CO_2 fixation in
211 continuous, saturating light. Note, that in spite of the ongoing controversy on how PGRL1 is
212 involved in CEF [37], a clear integration is observed between PGRL1-controled CEF, PCEF and
213 CMEF in which these different pathways can compensate each other in powering
214 photosynthesis. Importantly, we observed similar effects on net O_2 and CO_2 exchange (**Sup**
215 **Fig. S7**), thus showing that all effects measured on net photosynthesis correspond to changes
216 in CO_2 fixation and eventually biomass production and growth (**Fig. 4 C**).
217 Some compensation between CEF, PCEF, and CMEF has been previously reported; a
218 *Chlamydomonas* PGRL1-deficient strain exhibits increased CMEF and PCEF [25] and mutants
219 of complexes I and III show enhanced rates of CEF [38]. We observed an elevated CMEF in the
220 absence of FLV (**Fig. 4 A, B**) with a higher level of terminal oxidases associated with CMEF

221 (**Sup Fig. 6**), corroborating cross-compensation among all three mechanisms of electron flow.
222 In diatoms, while CMEF is considered to be a major driver of CO_2 fixation, inhibition of CMEF
223 only leads to a ~20% decrease of the PSII yield [26], which might also reflect compensation by
224 CEF. We also conclude, in agreement with previous studies that the NDA2-mediated CEF
225 represents a small fraction of alternative electron flow [37,39], and while it may contribute to some
226 extent under specific conditions [15], it is not sufficient by itself to sustain CO_2 fixation (**Fig. 2**
227 **B**).

228 It is important to note here that the quantification of each pathway relies on the
229 assumption that inhibiting one pathway (CMEF or PCEF) does not affect the flow through the
230 others. Because this assumption is likely not valid, we used two independent methods to
231 quantify electron flows (**Fig. 4 A, B**), one likely overestimating CMEF (using *flvB* mutants),
232 the other likely overestimating PCEF (using inhibitors of respiration), whereas both approaches
233 would likely overestimate CEF. The actual contribution of each pathway in the absence of
234 complications introduced with the use of mutations or inhibitors is likely to lie somewhere
235 between these two extreme estimations, which would suggest a rather balanced contribution of
236 each pathway in the conditions of our experiments. Therefore, if CEF, PCEF and CMEF can
237 all contribute to supplying energy for CO_2 fixation, it is likely that a different mix of these
238 pathways may be involved in different environmental conditions, each pathway being possibly
239 more advantageous in specific conditions.

240

241 ***The e^- quantum yield, a new tool to evaluate the efficiency of electron transport pathways.***

242 In support to LEF, a combination of PGRL1-controled CEF and PCEF cannot sustain more than
243 80% of maximal CO_2 fixation (**Fig. 3 E**) whereas each individual flux can help sustain 60% of
244 it (**Fig. 3 F**). This suggests the existence of an intrinsic limitation of the flow of electrons
245 through the photosynthetic electron transport chain, which is likely due to a *pmf*-induced
246 photosynthetic control occurring at the cytochrome b_6f level [40,41]; an elevated *pmf* elicits a block
247 in electron flow across the complex. Engaging an electron pathway with a high e^- quantum
248 yield, such as CMEF, might be a way to avoid this limitation since less electrons would be
249 needed to power the same level of CO_2 fixation. Such a strategy seems to be used by diatoms
250 [26] and mosses [42].

251 Throughout the green lineage, the nature and activity of alternative electron flows are
252 quite different. For example, angiosperms lack FLV-dependent PCEF [43], harbour a NDH-1-
253 dependent CEF pathway [10] and have a weakly active CMEF [23]. Since the NDH-1 dependent
254 CEF translocates $4H^+/e^-$ [44], its e^- quantum yield is close to that of CMEF, strongly suggesting

that in angiosperms the NDH-1 complex can compensate when the CMEF capacity is diminished. The latter is illustrated by the poor growth of *Arabidopsis thaliana* mutants impaired in both CEF pathways (PGR and NDH-1) [8]. Because of the number of key proteins and biochemical reactions involved in CMEF, its high e^- quantum yield may not be as rapidly accessible as CEF or PCEF during environmental fluctuations. While under light limiting conditions a high e^- quantum yield pathway might be advantageous, a less efficient pathway would contribute to the safe dissipation of excess absorbed light energy and diminished reactive oxygen production at saturating light intensities. Overall, it remains to be determined to what extent harbouring a palette of alternative electron flows with varying quantum yields and likely different time responses, is critical for sustaining photosynthetic performance under dynamic conditions in nature.

Additional energy cost of photosynthesis.

Allen previously estimated that a PCEF representing only 16*%-LEF* would be sufficient, in addition to LEF, to satisfy the ATP and NADPH requirement of the CBB cycle [45]. Our conclusions are strikingly different since we estimate that if only PCEF was active, it would have to represent 54*%-LEF* to sustain CO_2 fixation. This discrepancy may reflect the fact that the actual metabolic cost of CO_2 fixation exceeds the ATP requirement of the CBB cycle. This may result from the involvement of additional ATP-consuming metabolic pathways or transporters, or to the presence of proton leakages from energized membranes. In addition, in natural environments, either terrestrial or aquatic, CO_2 fixation is further limited by the concentration of atmospheric CO_2, which can trigger photorespiration in C_3 plants or induction of the carbon concentration mechanisms in C_4 plants and algae. All these mechanisms would require additional energy for their activities [30,46-48], making alternative electron pathways of photosynthesis even more critical for sustaining plant and algal CO_2 capture.

Acknowledgements

The authors acknowledge the constructive comments on the manuscript from Dr. Joe Berry, Dr. Jennifer Johnson, Evan Saldivar, and Leron Perez. This work was supported by the Carnegie Institution for Science (AB, AG), and the ANR grants OTOLHYD n°ANR-18-CE05-0029 and AlgalCCM n°ANR-22-CE44-0023-01 (GP). This work was also in part supported by DOE award DE-SC0019417 to AG.

H^+/e^-	CEF	PCEF	CMEF via AOX	CMEF via III/IV
Thylakoid	**2**	**3**	**2.5**	**2.5**
Inner mitochondrial membrane	**0**	**0**	**2.5**	**5.5**
Total	**2**	**3**	**5**	**8**

Table 1. Number of protons translocated per electron for each electron flow in the thylakoid and mitochondrial membranes. H^+/e^- coupling efficiencies of the photosynthetic and mitochondrial electron transport chain were estimated based on previously published data [35, 49]. Assuming that protons that are translocated across the thylakoid or inner mitochondrial membrane equally contribute to ATP production (*i.e.* no difference in the H^+ leakage of membranes), then AOX and the complex III-IV pathways would respectively require 5/3 and 8/3 times less electrons than PCEF per ATP produced.

Figure legend:

Figure 1. Electron transport pathways operating during oxygenic photosynthesis and their role in ATP generation. Linear electron flow (LEF) operates from PSII to PSI and reduces $NADP^+$ to NADPH using electrons from water. It also generates a *pmf* across the thylakoid membrane composed of a proton gradient (ΔpH) and electrical gradient (ΔΨ); the *pmf* is used by the ATPase to generate ATP. Cyclic electron flow (CEF) and pseudo cyclic electron flow (PCEF) both contribute to the generation of the *pmf* but do not produce reducing equivalents since the e^- used for PCEF reduce O_2 to water. Chloroplast to mitochondria electron flow (CMEF) encompasses multiple metabolic pathways by which reductants generated in the chloroplast is shuttled to the mitochondria and converted into ATP by the mitochondrial electron transport chain. NADPH and ATP generated by these different pathways are eventually used for transforming CO_2 into biomass, which reflects net photosynthesis. Other abbreviations: AOX, alternative oxidase; ATP, adenosine triphosphate; CBB, Calvin Benson Bassham; FDX, ferredoxin; FLVs, flavodiiron proteins; FNR, ferredoxin-$NADP^+$ reductase; Myxo, myxothiazol; NADPH, reduced form of nicotinamide adenine dinucleotide phosphate; PS, photosystem; PGR5/L1, proton gradient generation 5/like-1; SHAM, salicyl hydroxamic acid.

Figure 2. Dependence of photosynthesis on CEF, PCEF and CMEF. A, B, O_2 exchange rates upon a dark to light transition in WT2 (**A**) and *pgrl1 flvB-1* (**B**). At t=6min, mitochondrial respiration inhibitors myxothiazol (2.5 μM) and salicylhydroxamic acid (SHAM, 400 μM) were added to the reaction. Shown are representative traces of $n = 3$ biologically independent samples. **C and D**, Net O_2 evolution in *pgrl1 flvB-1* and *pgrl1 flvB*-3 and their control strains (WT2 and WT3) in the absence (control) or presence (Myxo & SHAM) of myxothiazol (2.5 μM) and salicylhydroxamic acid (SHAM, 400 μM) in cells grown in air (**C**) or in 2% CO_2-

enriched air (**D**). Values are taken after 9 min of illumination upon a dark to light transitions. Bars show the average and dots show individual replicates ($n = 3$ biologically independent samples). Typical experiments used to extract these data are shown in **Sup. Fig. S2**. **E** and **F**, Cross section images showing subcellular localization of mitochondria-localized Clover (yellow fluorescence) in *pgrl1 flvB-1* and a control strain (WT2), grown in air (**E**) or 2% CO_2-enriched air (**F**). Images are representative of 2 independent experiments. Scale bar: 10 µm. Brightfield, Clover fluorescence, Chlorophyll autofluorescence and Clover/Chlorophyll merge signals are shown. Images are representative of 2 experiments. Scale bar: 10 µm.

Figure 3. Relative efficiencies of CEF, PCEF and CMEF in energizing net photosynthesis. A-D, Net O_2 evolution measured during a dark to light transition in *flvB* (**A**), *pgrl1* (B), *pgrl1 flvB*-2 (**C**, **D**), treated (gray dots) or not treated (black dots) with both myxothiazol (Myxo, 2.5 μM) and salicylhydroxamic acid (SHAM, 400 μM) (**A, B**), or with only one inhibitor (**C,D**). Shown are representative traces of 3 biological replicates. **E**, Relative V_{max} measured when a given set of alternative electron pathways are active after treatment with myxothiazol (Myxo, 2.5 μM), salicylhydroxamic acid (SHAM, 400 μM) or both inhibitors; CEF (blue, *flvB* treated with Myxo and SHAM), PCEF (green, *pgrl1* treated with Myxo and SHAM), CEF&PCEF (dark, control strains treated with Myxo and SHAM), CMEF via AOX (purple, *pgrl1 flvB* treated with Myxo), CMEF via III/IV (red, *pgrl1 flvB* treated with SHAM). **F,** Electron quantum yield of PCEF (green), CMEF via AOX (purple), CMEF via III/IV (red), CMEF (pink) and CEF (dotted line). Similar electron quantum yields were also determined for PCEF in 2% CO_2-grown cells and a slightly lower quantum yield for CMEF (**Sup Fig. S9 D**). **G**, Electron flux relative to PCEF required to power similar levels of net photosynthesis when relying on a single pathway. Data shown are individual extrapolations based on measured electron quantum yields. In **E, F** and **G,** bars show the average and dots show individual replicates ($n \geq 3$ biologically independent sample).

Figure 4. Contribution of CEF, PCEF and CMEF to the electron flow, net photosynthesis and growth. A Electron flow through PCEF, CEF and CMEF relative to LEF were determined in the wildtype strain CC-4533 by two different methods, one based on the use of inhibitors (inhib) the other on mutants (mut). Data used for these calculations are the same as for **Fig. 2 C** and **Sup Fig. 2**. **B** Proportion of net photosynthesis powered by each electron flow (PCEF, CEF and CMEF) in the control strain CC-4533 as measured by the inhibition (inhib) or mutant (mut) method. CC-4533 was chosen because it is the control strain for *flvB* and is therefore the only strain where both methods could be used. Data used for these calculations are the same as for **A**. In **A** and **B,** bars show the average and dots show individual replicates (n=3 biologically independent sample). **C**, Growth tests for *flvB* and *pgrl1* mutants, their corresponding control strains (CC-4533 and 137AH, respectively) and double mutants (*pgrl1 flvB-1 and pgrl1 flv-3*) and their corresponding control strains (WT2 and 3). Cells were spotted on plates containing minimal medium at pH 7.2 and grown under continuous illumination (60 µmol photon m^{-2} s^{-1}) in the absence (upper panel) or presence (lower panel) of 2.5µM Myxothiazol (Myxo) in air enriched at 2% CO_2. Spots shown are representative of 10 independent experiments.

363 **Material and Methods**

364 **Strains and growing conditions.** *Chlamydomonas flvB* and *pgrl1* single mutants and their
365 respective parental strains CC-4533 (for *flvB*), 137AH (for *pgrl1*) where previously
366 described[11,19]. *flvB pgrl1*-1, -2 and -3 double mutant and their respective sibling strains WT2
367 and WT3 (used here as control strains) have been described previously[30] and are all from the
368 progeny of a crossing of *flvB* and *pgrl1* performed in[30]. Because *pgrl1 flvB* double mutants were
369 obtained by crossing the two single mutants which have different genetic backgrounds (as
370 described in [30]), the control strains used are siblings that resulted from the cross and that
371 contained wild-type copies and levels of the FLVB and PGRL1 proteins. *pgrl1-2* is a mutant
372 impaired in accumulation of the PGRL1 protein originating from crossing *flvB* and *pgrl1*
373 performed in [30]. All strains were grown photo-autotrophically in 125-mL flasks with cotton
374 stoppers at 25 °C in a buffered minimal medium (20 mM MOPS pH 7.2) under constant
375 illumination (80 µmol photons m^{-2} s^{-1}) either under ambient CO_2 or 2% CO_2 in air. Amongst
376 *pgrl1 flvB* double mutants and their control strains already described [30], *pgrl1 flvB*-1 and *pgrl1*
377 *flvB*-3 and WT2 and 3, respectively, were used for physiological measurements since their
378 maximal photosynthesis was representative of other double mutants and control strains [30]. All
379 strains used in this study are available under the same names used here (except for *flvB* which
380 is available as *flvB-21*) at the Chlamydomonas Resource Center (www.chlamycollection.org).
381 **Gas exchange measurements.** Gas exchange rates were measured using membrane inlet mass
382 spectrometry (MIMS). Cells grown in air enriched or not at 2% CO_2 were collected during the
383 exponential phase by centrifugation at 450 g for 3 min and resuspended in 1.5 mL of fresh
384 buffered minimal medium (pH 7.2) at 10 µg chlorophyll mL^{-1}. The cell suspension was then
385 placed in the MIMS reaction vessel, 2 mL of ^{18}O-enriched O_2 (97% ^{18}O Eurisop, France) were
386 bubbled in the suspension. After closing the vessel, gas exchange was recorded during a dark
387 to light transition (2,000 µmol photons m^{-2} s^{-1}; green LEDs). Calculations of gross and net
388 photosynthesis were done using the MIMS analysis software as previously described[31]. In some
389 experiments salicyl hydroxamic acid (SHAM, 400 µM final concentration) and/or myxothizol
390 (Myxo, 2.5 µM final concentration) were added 1 min before the beginning of the
391 measurements, except for the data presented in **Fig. 2A**, **B** where inhibitors were added during
392 the measurement. All Net O_2, Net CO_2, e^- quantum yield, e^- flow and Net photosynthesis
393 sustained shown as histograms in **Figs. 2, 3, 4** and **Sup. Figs. 1, 7, 9, 11** are based on
394 measurements after 9 minutes of illumination.

395 **Clover Expressing cells.** 137AH, WT2, *pgrl1*, *flvB*, *pgrl1flvB*-1 and -2 expressing the
396 mitochondria targeted fluorophore Clover (mito-Clover) were generated as described in [50].
397 Briefly, cells were transformed with a linearized plasmid encoding mito-Clover and a
398 hygromycin-resistance cassette using the Max Efficiency Reagent (Invitrogen). Resistant
399 clones to hygromycin were screened for Clover fluorescence using a M1000 Tecan plate reader
400 (Excitation: 488/7 nm; Emission: 515/10 nm) and mitochondrial signal was checked by
401 confocal microscopy. Selected clones were grown at 80 µmol photons m^{-2} s^{-1} in 25 mL minimal
402 medium in 125 mL flasks, in the presence of either normal or 2% CO_2-enriched air until they
403 reached a density of ~10 µg chlorophyll mL^{-1}. An aliquot of each culture was then briefly
404 concentrated by centrifugation at 1,500g and cells layered on a 18-well microscope slide.
405 Images were acquired using a TCS SP8 confocal laser-scanning microscope (Leica) and a ×63
406 objective. Acquisition settings were as follows: Clover excitation 488 nm, emission 500-547
407 nm; Chlorophyll excitation 488 nm, emission 694-733 nm. For homogeneity and clarity, signal
408 intensities of each channel were adjusted using the Fiji software.
409 **Growth tests.** The different *Chlamydomonas* strains were cultivated at air level of CO_2 under
410 moderate light (80 µmol photons m^{-2} s^{-1}) at 25 °C. Cells were collected during exponential
411 growth and diluted in fresh minimal medium to 0.125, 0.625 or 2.5 10^6 cells mL^{-1}. Seven-
412 microlitre drops were spotted on 2% Agar plates of minimal medium (buffered with 20mM
413 MOPS pH 7.2) with or without myxothiazol (2.5µM final concentration) and exposed to air
414 enriched with 2% CO_2. Homogeneous light was supplied by LED panels, the different light
415 intensities were obtained with various dimmers. Temperature was maintained at 25 °C at the
416 level of plates by means of fans.
417 **Electron quantum yield calculation.** The e^- quantum yield of a given alternative electron
418 pathway is defined as the proportion of electrons generated downstream PSI that are used for
419 net photosynthesis when only this alternative electron pathway is active, following this
420 equation:

421 $$(1)\ e^- quantum\ yield = \frac{e^-(net\ photosynthesis)}{e^-(net\ photosynthesis) + e^-(alternative\ pathway)}$$

422 Where e^-(net photosynthesis) is the flux of photosynthetic electrons directly used as reductants
423 for net photosynthesis and e^-(alternative pathway) is the flux of photosynthetic electrons
424 through an alternative pathway. Because for PCEF and CMEF the sum of e^-(alternative
425 pathway) and e^-(net photosynthesis) equals gross photosynthesis, electron quantum yields of
426 PCEF and CMEF were quantified using gross and net O_2 evolution in mutants harbouring: only
427 PCEF (*pgrl1* and *pgrl1-2* mutants treated with Myxo and SHAM), or only the AOX or the

complex III/IV pathway of CMEF (*pgrl1 flvB*-1 and 3 mutants treated with Myxo or SHAM, respectively). The electron quantum yield was then calculated for each pathway using the following equation:

$$(2)\ e^{-}quantum\ yield = \frac{net\ O_2 evolution}{gross\ O_2 evolution}$$

The theoretical electron quantum yield of CEF was calculated based on the assumption that CEF translocates 1.5 less protons per electron across the thylakoid membranes than PCEF and that this is the driving force leading to net photosynthesis energization. Note that this later assumption is well supported by the independent results from **Fig. 3 G** showing that the relative electron quantum yield of CMEF pathways and PCEF corresponds to their relative capacity at translocating protons across membranes. Hence, for the same net photosynthesis powered, CEF should be 1.5 times higher than PCEF, and the electron quantum yields of CEF could be written as:

$$(3)\qquad e^{-}quantum\ yield\ (CEF) = \frac{e^{-}(net\ in\ pgrl1\ Myxo\ SHAM)}{e^{-}(net\ in\ pgrl1\ Myxo\ SHAM)+e^{-}(PCEF)\times 1.5}$$

Where e^{-}(net in *pgrl1* Myxo SHAM) is the net photosynthesis measured in the *pgrl1* mutant treated with Myxo and SHAM (hence having only PCEF active) and e^{-} (PCEF) being the O_2 uptake rate in the same strain and condition.

Based on equation (1), we can rewrite e^{-}(PCEF) as:

$$(4)\qquad e^{-}(PCEF) = \frac{(1-e^{-}quantum\ yield(PCEF))}{e^{-}quantum\ yield(PCEF)} \times\ e^{-}(net\ in\ pgrl1\ Myxo\ SHAM)$$

Hence, combining (3) and (4):

$$(5)\qquad e^{-}quantum\ yield\ (CEF) = \frac{e^{-}quantum\ yield\ (PCEF)}{1.5-\frac{e^{-}quantum\ yield\ (PCEF)}{2}}$$

The electron quantum yield of CEF shown in **Fig. 3** is using equation (5) with the average electron quantum yield of PCEF. Note that the quantifications of the e^{-} quantum yield in *Chlamydomonas* assumes that removing two pathways (elimination of CEF and CMEF in the *pgrl1* mutant treated with inhibitors of respiration, and CEF and PCEF in the *pgrl1 flvB* double mutants) makes CO_2 fixation dependent only on the third pathway. This dependency is supported by the finding that the *pgrl1 flvB* double mutant treated with inhibitors of respiration are unable to support any CO_2 fixation, which also support the hypothesis that the contribution of other pathways, such as the NDA2-dependent CEF, is marginal.

460 **Calculation of electron flows via each pathway and their contribution to net**
461 **photosynthesis in wildtype strains.** The electron flow through PCEF and CMEF were deduced
462 on wildtype strain using two independent methods based on measurements of gross O_2 uptake
463 made in **Sup. Fig. 2 and 3**. In the so called "mutant" method, CMEF was quantified as being
464 the gross O_2 uptake measured in the *flvB* mutant. Then, PCEF was quantified by subtracting the
465 CMEF to the O_2 uptake of CC-4533 (**Sup. Fig. S10**). This method was only used for CC-4533
466 since it is the only control strain for the *flvB* mutant. In the so called "inhibitor" method, PCEF
467 was quantified as being the gross O_2 uptake remaining in control strains treated with SHAM
468 and Myxo. Then, CMEF was quantified by subtracting the PCEF to the O_2 uptake in the same
469 untreated control strain (**Sup. Fig. S10**). The calculated electron flows of PCEF and CMEF
470 were then used for each strain to quantify the net photosynthesis powered by each of them
471 following the equations derived from (1):

472 $$e^{-}(net\ by\ AEF) = e^{-}(AEF)\frac{e^{-}quantum\ yield\ (AEF)}{1 - e^{-}quantum\ yield\ (AEF)}$$

473

474 Where e^- (net by AEF) is the net photosynthesis sustained by a specific alternative electron
475 flow, e^-(AEF) being the electron flow through this AEF and e^- quantum yield (AEF) being the
476 electron quantum yield of this alternative electron flow.
477 The total of net photosynthesis powered in a strain by PCEF and CMEF was then compared to
478 the measured net photosynthesis in this same strain to quantify the "missing" net photosynthesis
479 that had to be powered by CEF. Then the electron flow through CEF (e^-(CEF)) was calculated
480 by the following equation derived from (1):

481 $$e^{-}(CEF) = e^{-}(missing\ net)\frac{1 - e^{-}quantum\ yield\ (CEF)}{e^{-}quantum\ yield\ (CEF)}$$

482 Where e^-(missing net) is the calculated net photosynthesis that is not powered by PCEF and
483 CMEF and e^- quantum yield (CEF) being the electron quantum yield of CEF.
484

485 **Protein extraction and Immunodetection.** Cells were harvested by centrifugation at 1,000g
486 for 5 minutes. Total cellular protein was extracted by heating the cell pellet at 100°C for one
487 minute using an extraction aqueous solution composed of 1% SDS, 100 mM DTT, 1mM
488 Aminocaproic acid, and 1mM benzamidine hydrochloride buffered with 60mM Tris (pH 6.8).
489 The resulting cell lysate was then centrifuged at 10,000 g for 5 minutes to obtain the
490 supernatant. The supernatant was subsequently incubated with acetone (80% final
491 concentration) at -20°C for 1 hour. The protein pellet was collected by centrifugation at 5,000

492 g for 5 minutes and stored in aqueous solution containing 1% SDS, 5 mM DTT and buffered
493 with 60mM Tris (pH 6.8). Protein content was estimated (Microplate BCA protein assay Kit-
494 reducing agent compatible, Thermo Scientific) with bovine serum albumin as the standard.
495 Protein extracts (10 µg protein) were loaded on a 12% SDS-PAGE gel and run for 1h at 150V
496 in Tris-glycine SDS buffer and transferred onto a nitrocellulose membrane using semi-dry
497 transfer (Transblot turbo, Biorad). Immunoblot detection was performed using antibodies raised
498 against FlvB (1:1,000)[19], and Pgrl1 (1:5,000)[11]. Other antibodies against AOX1 (1:10,000)
499 (AS06 152), COXIIB (1:10,000) (AS06 151) were obtained from Agrisera
500 (https://www.agrisera.com/). An anti-rabbit HRP-conjugated antibody (1:50,000) (AS09 602)
501 was used as a secondary antibody for immunodetection. Precision Plus Protein Dual Color
502 Standards (Biorad) was used as the molecular weight marker. Uncropped and unprocessed
503 scans of the blots shown in this study are visible in source data.
504
505 **Data Availability.** Genes studied in this article can be found on https://phytozome-
506 next.jgi.doe.gov/ under the loci Cre12.g531900 (FLVA), Cre16.g691800 (FLVB),
507 Cre07.g340200 (PGRL1), Cre09.g395950 (AOX1), Cre03.g169550 (AOX2) and
508 Cre01.g049500 (COXIIB).
509

510 # References

511

512 1 IPCC. *Climate Change 2021: The Physical Science Basis. Contribution of Working*
513 *Group I to the Sixth Assessment Report of the Intergovernmental Panel on Climate*
514 *Change* (Cambridge University Press, 2021).
515 2 Johnson, X. & Alric, J. Central carbon metabolism and electron transport in
516 *Chlamydomonas reinhardtii*: metabolic constraints for carbon partitioning between oil
517 and starch. *Eukaryotic Cell* **12**, 776-793, doi:10.1128/ec.00318-12 (2013).
518 3 Allen, J. F. Cyclic, pseudocyclic and noncyclic photophosphorylation: new links in the
519 chain. *Trends Plant Sci.* **8**, 15-19, doi:10.1016/s1360-1385(02)00006-7 (2003).
520 4 Arnon, D. I. Conversion of light into chemical energy in photosynthesis. *Nature* **184**,
521 10-21, doi:10.1038/184010a0 (1959).
522 5 Arnon, D. I. The discovery of photosynthetic phosphorylation. *Trends Plant Sci* **9**, 258-
523 262, doi:https://doi.org/10.1016/0968-0004(84)90159-2 (1984).
524 6 Munekage, Y. *et al.* PGR5 is involved in cyclic electron flow around photosystem I and
525 is essential for photoprotection in *Arabidopsis*. *Cell* **110**, 361-371,
526 doi:https://doi.org/10.1016/S0092-8674(02)00867-X (2002).
527 7 DalCorso, G. *et al.* A complex containing PGRL1 and PGR5 is involved in the switch
528 between linear and cyclic electron flow in *Arabidopsis*. *Cell* **132**, 273-285,
529 doi:10.1016/j.cell.2007.12.028 (2008).

8 Munekage, Y. *et al.* Cyclic electron flow around photosystem I is essential for photosynthesis. *Nature* **429**, 579-582, doi:10.1038/nature02598 (2004).

9 Joët, T., Cournac, L., Horvath, E. M., Medgyesy, P. & Peltier, G. Increased sensitivity of photosynthesis to antimycin A induced by inactivation of the chloroplast ndhB gene. evidence for a participation of the NADH-dehydrogenase complex to cyclic electron flow around photosystem I. *Plant Physiol.* **125**, 1919-1929, doi:10.1104/pp.125.4.1919 (2001).

10 Peltier, G., Aro, E. M. & Shikanai, T. NDH-1 and NDH-2 plastoquinone reductases in oxygenic photosynthesis. *Ann. Rev. Plant Biol.* **67**, 55-80, doi:10.1146/annurev-arplant-043014-114752 (2016).

11 Tolleter, D. *et al.* Control of hydrogen photoproduction by the proton gradient generated by cyclic electron flow in *Chlamydomonas reinhardtii*. *Plant Cell* **23**, 2619-2630, doi:10.1105/tpc.111.086876 (2011).

12 Johnson, X. *et al.* Proton Gradient Regulation 5-mediated cyclic electron flow under ATP- or redox-limited conditions: A study of Δ*ATPase pgr5* and *ΔrbcL pgr5* mutants in the green alga *Chlamydomonas reinhardtii*. *Plant Physiol.* **165**, 438-452, doi:10.1104/pp.113.233593 (2014).

13 Desplats, C. *et al.* Characterization of Nda2, a plastoquinone-reducing type II NAD(P)H dehydrogenase in *Chlamydomonas* chloroplasts. *J. Biol. Chem.* **284**, 4148-4157, doi:10.1074/jbc.M804546200 (2009).

14 Jans, F. *et al.* A type II NAD(P) H dehydrogenase mediates light-independent plastoquinone reduction in the chloroplast of *Chlamydomonas*. *Proc. Natl. Acad. Sci. U.S.A.* **105**, 20546-20551, doi:10.1073/pnas.0806896105 (2008).

15 Saroussi, S. I., Wittkopp, T. M. & Grossman, A. R. The Type II NADPH dehydrogenase facilitates cyclic electron flow, energy-dependent quenching, and chlororespiratory metabolism during acclimation of *Chlamydomonas reinhardtii* to nitrogen deprivation *Plant Physiol.* **170**, 1975-1988, doi:10.1104/pp.15.02014 (2016).

16 Peltier, G. & Schmidt, G. W. Chlororespiration - an adaptation to nitrogen deficiency in *Chlamydomonas reinhardtii*. *Proc. Natl. Acad. Sci. USA* **88**, 4791-4795, doi:10.1073/pnas.88.11.4791 (1991).

17 Helman, Y. *et al.* Genes encoding a-type flavoproteins are essential for photoreduction of O_2 in cyanobacteria. *Curr. Biol.* **13**, 230-235 (2003).

18 Allahverdiyeva, Y. *et al.* Flavodiiron proteins Flv1 and Flv3 enable cyanobacterial growth and photosynthesis under fluctuating light. *Proc. Natl. Acad. Sci. U.S.A.* **110**, 4111-4116, doi:10.1073/pnas.1221194110 (2013).

19 Chaux, F. *et al.* Flavodiiron proteins promote fast and transient O_2 photoreduction in Chlamydomonas. *Plant Physiol.* **174**, 1825-1836, doi:10.1104/pp.17.00421 (2017).

20 Gerotto, C. *et al.* Flavodiiron proteins act as safety valve for electrons in Physcomitrella patens. *Proc. Nat. Acad. Sci. U.S.A.* **113**, 12322-12327, doi:10.1073/pnas.1606685113 (2016).

21 Shimakawa, G. *et al.* The Liverwort, Marchantia, drives alternative electron flow using a flavodiiron protein to protect PSI. *Plant Physiol.* **173**, 1636-1647, doi:10.1104/pp.16.01038 (2017).

22 Ilík, P. *et al.* Alternative electron transport mediated by flavodiiron proteins is operational in organisms from cyanobacteria up to gymnosperms. *New Phytol.* **214**, 967-972, doi:10.1111/nph.14536 (2017).

23 Raghavendra, A. S. & Padmasree, K. Beneficial interactions of mitochondrial metabolism with photosynthetic carbon assimilation. *Trends Plant Sci.* **8**, 546-553, doi:https://doi.org/10.1016/j.tplants.2003.09.015 (2003).

24 Lemaire, C., Wollman, F. A. & Bennoun, P. Restoration of phototrophic growth in a mutant of *Chlamydomonas reinhardtii* in which the chloroplast *atpB* gene of the ATP synthase has a deletion: an example of mitochondria-dependent photosynthesis. *Proc. Natl. Acad. Sci. USA* **85**, 1344-1348 (1988).

25 Dang, K. V. *et al.* Combined increases in mitochondrial cooperation and oxygen photoreduction compensate for deficiency in cyclic electron flow in *Chlamydomonas reinhardtii*. *Plant Cell* **26**, 3036-3050, doi:10.1105/tpc.114.126375 (2014).

26 Bailleul, B. *et al.* Energetic coupling between plastids and mitochondria drives CO_2 assimilation in diatoms. *Nature* **524**, 366, doi:10.1038/nature14599 (2015).

27 Alric, J. & Johnson, X. Alternative electron transport pathways in photosynthesis: a confluence of regulation. *Curr. Op. Plant. Biol.* **37**, 78-86, doi:https://doi.org/10.1016/j.pbi.2017.03.014 (2017).

28 Alboresi, A., Storti, M. & Morosinotto, T. Balancing protection and efficiency in the regulation of photosynthetic electron transport across plant evolution. *New Phytol.* **221**, 105-109, doi:10.1111/nph.15372 (2019).

29 Kaye, Y. *et al.* The mitochondrial alternative oxidase from *Chlamydomonas reinhardtii* enables survival in high light. *J. Biol. Chem.* **294**, 1380-1395, doi:10.1074/jbc.RA118.004667 (2019).

30 Burlacot, A. *et al.* Alternative photosynthesis pathways drive the algal CO_2 concentrating mechanism. *Nature*, doi:https://doi.org/10.1038/s41586-022-04662-9 (2022).

31 Burlacot, A., Burlacot, F., Li-Beisson, Y. & Peltier, G. Membrane Inlet Mass Spectrometry: A Powerful Tool for Algal Research. *Front. Plant. Sci.* **11**, doi:10.3389/fpls.2020.01302 (2020).

32 Cournac, L. *et al. In vivo* interactions between photosynthesis, mitorespiration, and chlororespiration in *Chlamydomonas reinhardtii*. *Plant Physiol.* **129**, 1921-1928, doi:10.1104/pp.001636 (2002).

33 Geraghty, A. M. & Spalding, M. H. Molecular and structural changes in *Chlamydomonas* under limiting CO_2 (a possible mitochondrial role in adaptation). **111**, 1339-1347, doi:10.1104/pp.111.4.1339 (1996).

34 Burlacot, A. & Peltier, G. Energy crosstalk between photosynthesis and the algal CCM. *Trends Plant Sci.*, doi:https://doi.org/10.1016/j.tplants.2023.03.018 (2023).

35 Kramer, D. M. & Evans, J. R. The importance of energy balance in improving photosynthetic productivity. *Plant Physiol.* **155**, 70-78, doi:10.1104/pp.110.166652 (2011).

36 Tomaz, T. *et al.* Mitochondrial malate dehydrogenase lowers leaf respiration and alters photorespiration and plant growth in *Arabidopsis*. *Plant Physiol.* **154**, 1143-1157, doi:10.1104/pp.110.161612 (2010).

37 Nawrocki, W. J. *et al.* The mechanism of cyclic electron flow. *Biochim. Biophys. Acta Bioenerg.* **1860**, 433-438, doi:https://doi.org/10.1016/j.bbabio.2018.12.005 (2019).

38 Cardol, P. *et al.* Impaired respiration discloses the physiological significance of state transitions in *Chlamydomonas*. **106**, 15979-15984, doi:10.1073/pnas.0908111106 (2009).

39 Alric, J., Lavergne, J. & Rappaport, F. Redox and ATP control of photosynthetic cyclic electron flow in *Chlamydomonas reinhardtii* (I) aerobic conditions. *Biochim. Biophys. Acta* **1797**, 44-51 (2010).

40 Johnson, J. E. & Berry, J. A. The role of Cytochrome b6f in the control of steady-state photosynthesis: a conceptual and quantitative model. *Phot. Res.* **148**, 101-136, doi:10.1007/s11120-021-00840-4 (2021).

41 Malone, L. A., Proctor, M. S., Hitchcock, A., Hunter, C. N. & Johnson, M. P. Cytochrome b6f – Orchestrator of photosynthetic electron transfer. *Biochim. Biophys. Acta* **1862**, 148380, doi:https://doi.org/10.1016/j.bbabio.2021.148380 (2021).

42 Mellon, M. *et al.* Inactivation of mitochondrial complex I stimulates chloroplast ATPase in Physcomitrium patens. *Plant Physiol.* **187**, 931-946, doi:10.1093/plphys/kiab276 (2021).

43 Peltier, G., Tolleter, D., Billon, E. & Cournac, L. Auxiliary electron transport pathways in chloroplasts of microalgae. *Photosynth. Res.* **106**, 19-31 (2010).

44 Strand, D. D., Fisher, N. & Kramer, D. M. The higher plant plastid NAD(P)H dehydrogenase-like complex (NDH) is a high efficiency proton pump that increases ATP production by cyclic electron flow. *J. Biol. Chem.* **292**, 11850-11860, doi:10.1074/jbc.M116.770792 (2017).

45 Allen, J. F. Photosynthesis of ATP—Electrons, Proton Pumps, Rotors, and Poise. *Cell* **110**, 273-276, doi:https://doi.org/10.1016/S0092-8674(02)00870-X (2002).

46 Takabayashi, A., Kishine, M., Asada, K., Endo, T. & Sato, F. Differential use of two cyclic electron flows around photosystem I for driving CO_2-concentration mechanism in C4 photosynthesis. *Proc. Natl. Acad. Sci. USA* **102**, 16898-16903, doi:10.1073/pnas.0507095102 (2005).

47 Walker, B. J., Strand, D. D., Kramer, D. M. & Cousins, A. B. The response of cyclic electron flow around photosystem I to changes in photorespiration and nitrate assimilation *Plant Physiol.* **165**, 453-462, doi:10.1104/pp.114.238238 (2014).

48 Osmond, C. B. Photorespiration and photoinhibition: Some implications for the energetics of photosynthesis. *Biochim. Biophys. Acta* **639**, 77-98, doi:https://doi.org/10.1016/0304-4173(81)90006-9 (1981).

49 Wikström, M., Sharma, V., Kaila, V. R. I., Hosler, J. P. & Hummer, G. New Perspectives on Proton Pumping in Cellular Respiration. *Chem. Rev.* **115**, 2196-2221, doi:10.1021/cr500448t (2015).

50 Harmon, J. *et al.* Intelligent image-activated sorting of *Chlamydomonas reinhardtii* by mitochondrial localization. *Cytometry Part A* **101**, 1027-1034, doi:https://doi.org/10.1002/cyto.a.24661 (2022).

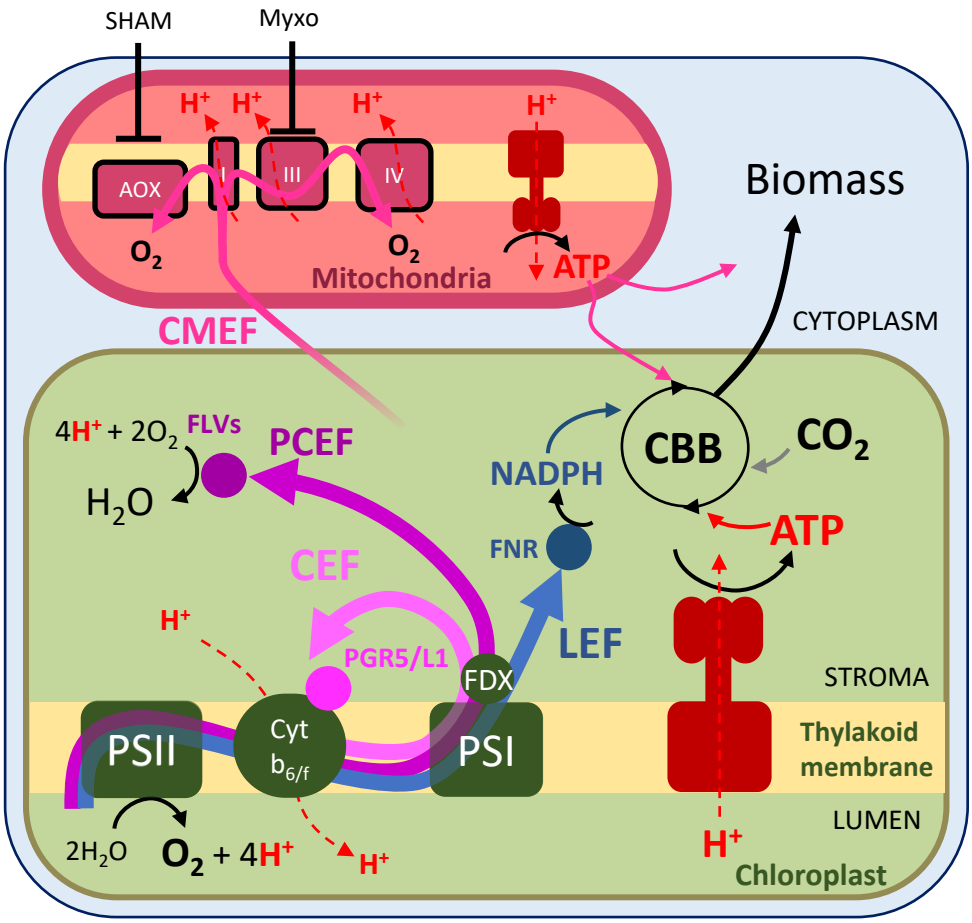

Figure 1. Electron transport pathways operating during oxygenic photosynthesis and their role in ATP generation. Linear electron flow (LEF) operates from PSII to PSI and reduces $NADP^+$ to NADPH using electrons from water. It also generates a *pmf* across the thylakoid membrane composed of a proton gradient (ΔpH) and electrical gradient (ΔΨ); the *pmf* is used by the ATPase to generate ATP. Cyclic electron flow (CEF) and pseudo cyclic electron flow (PCEF) both contribute to the generation of the *pmf* but do not produce reducing equivalents since the e^- used for PCEF reduce O_2 to water. Chloroplast to mitochondria electron flow (CMEF) encompasses multiple metabolic pathways by which reductants generated in the chloroplast is shuttled to the mitochondria and converted into ATP by the mitochondrial electron transport chain. NADPH and ATP generated by these different pathways are eventually used for transforming CO_2 into biomass, which reflects net photosynthesis. Other abbreviations: AOX, alternative oxidase; ATP, adenosine triphosphate; CBB, Calvin Benson Bassham; FDX, ferredoxin; FLVs, flavodiiron proteins; FNR, ferredoxin-$NADP^+$ reductase; Myxo, myxothiazol; NADPH, reduced form of nicotinamide adenine dinucleotide phosphate; PS, photosystem; PGR5/L1, proton gradient generation 5/like-1; SHAM, salicyl hydroxamic acid.

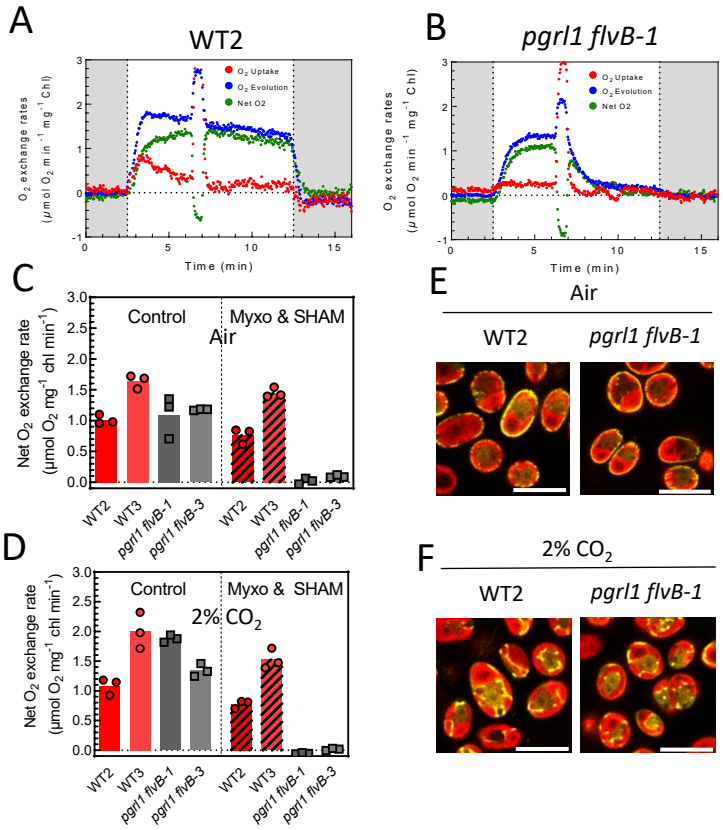

Figure 2. Dependence of photosynthesis on CEF, PCEF and CMEF. A, B, O_2 exchange rates upon a dark to light transition in WT2 (**A**) and *pgrl1 flvB-1* (**B**). At t=6min, mitochondrial respiration inhibitors myxothiazol (2.5 μM) and salicylhydroxamic acid (SHAM, 400 μM) were added to the reaction. Shown are representative traces of $n = 3$ biologically independent samples. **C and D**, Net O_2 evolution in *pgrl1 flvB-1* and *pgrl1 flvB*-3 and their control strains (WT2 and WT3) in the absence (control) or presence (Myxo & SHAM) of myxothiazol (2.5 μM) and salicylhydroxamic acid (SHAM, 400 μM) in cells grown in air (**C**) or in 2% CO_2-enriched air (**D**). Values are taken after 9 min of illumination upon a dark to light transitions. Bars show the average and dots show individual replicates ($n = 3$ biologically independent samples). Typical experiments used to extract these data are shown in **Sup. Fig. S2**. **E** and **F**, Cross section images showing subcellular localization of mitochondria-localized Clover (yellow fluorescence) in *pgrl1 flvB-1* and a control strain (WT2), grown in air (**E**) or 2% CO_2-enriched air (**F**). Images are representative of 2 independent experiments. Scale bar: 10 µm. Brightfield, Clover fluorescence, Chlorophyll autofluorescence and Clover/Chlorophyll merge signals are shown. Images are representative of 2 experiments. Scale bar: 10 µm.

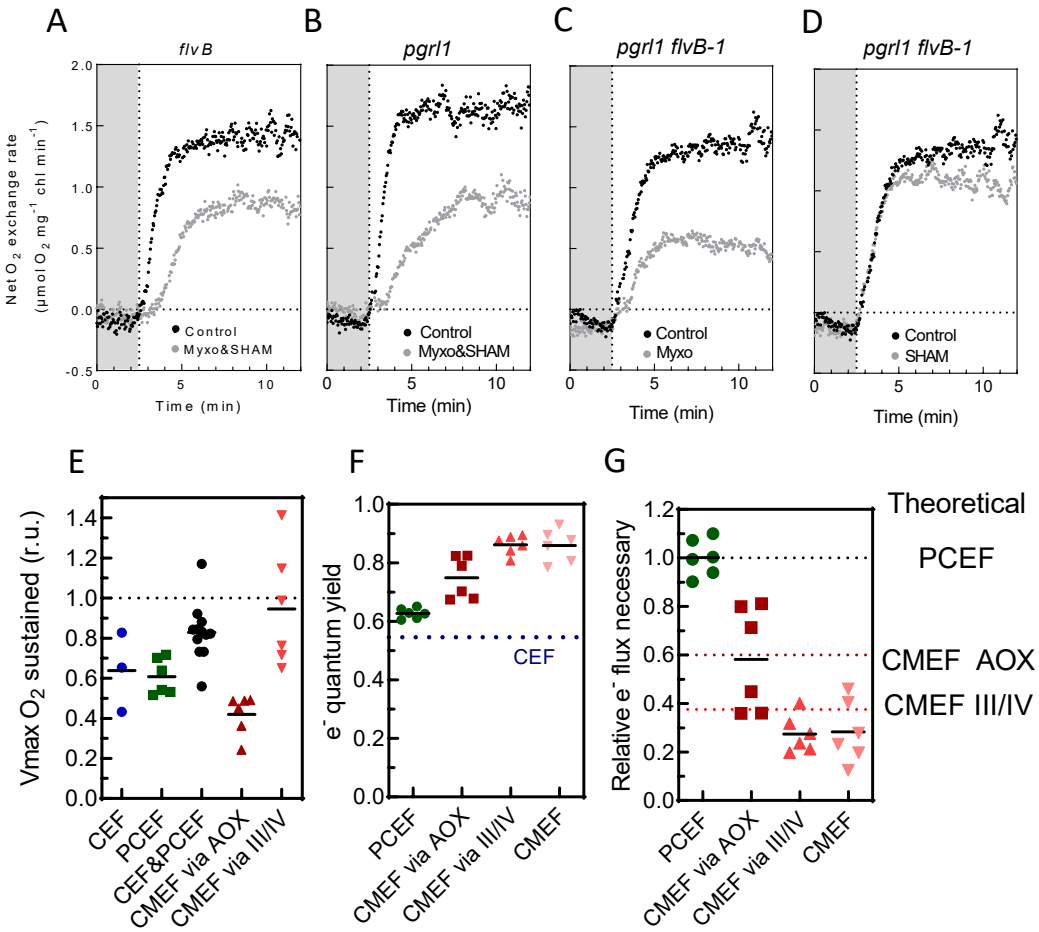

Figure 3. Relative efficiencies of CEF, PCEF and CMEF in energizing net photosynthesis. A-D, Net O_2 evolution measured during a dark to light transition in *flvB* (**A**), *pgrl1* (B), *pgrl1 flvB*-2 (**C**, **D**), treated (gray dots) or not treated (black dots) with both myxothiazol (Myxo, 2.5 μM) and salicylhydroxamic acid (SHAM, 400 μM) (**A, B**), or with only one inhibitor (**C,D**). Shown are representative traces of 3 biological replicates. **E**, Relative V_{max} measured when a given set of alternative electron pathways are active after treatment with myxothiazol (Myxo, 2.5 μM), salicylhydroxamic acid (SHAM, 400 μM) or both inhibitors; CEF (blue, *flvB* treated with Myxo and SHAM), PCEF (green, *pgrl1* treated with Myxo and SHAM), CEF&PCEF (dark, control strains treated with Myxo and SHAM), CMEF via AOX (purple, *pgrl1 flvB* treated with Myxo), CMEF via III/IV (red, *pgrl1 flvB* treated with SHAM). **F,** Electron quantum yield of PCEF (green), CMEF via AOX (purple), CMEF via III/IV (red), CMEF (pink) and CEF (dotted line). Similar electron quantum yields were also determined for PCEF in 2% CO_2-grown cells and a slightly lower quantum yield for CMEF (**Sup Fig. S9 D**). **G**, Electron flux relative to PCEF required to power similar levels of net photosynthesis when relying on a single pathway. Data shown are individual extrapolations based on measured electron quantum yields. In **E, F** and **G,** bars show the average and dots show individual replicates ($n \geq 3$ biologically independent sample).

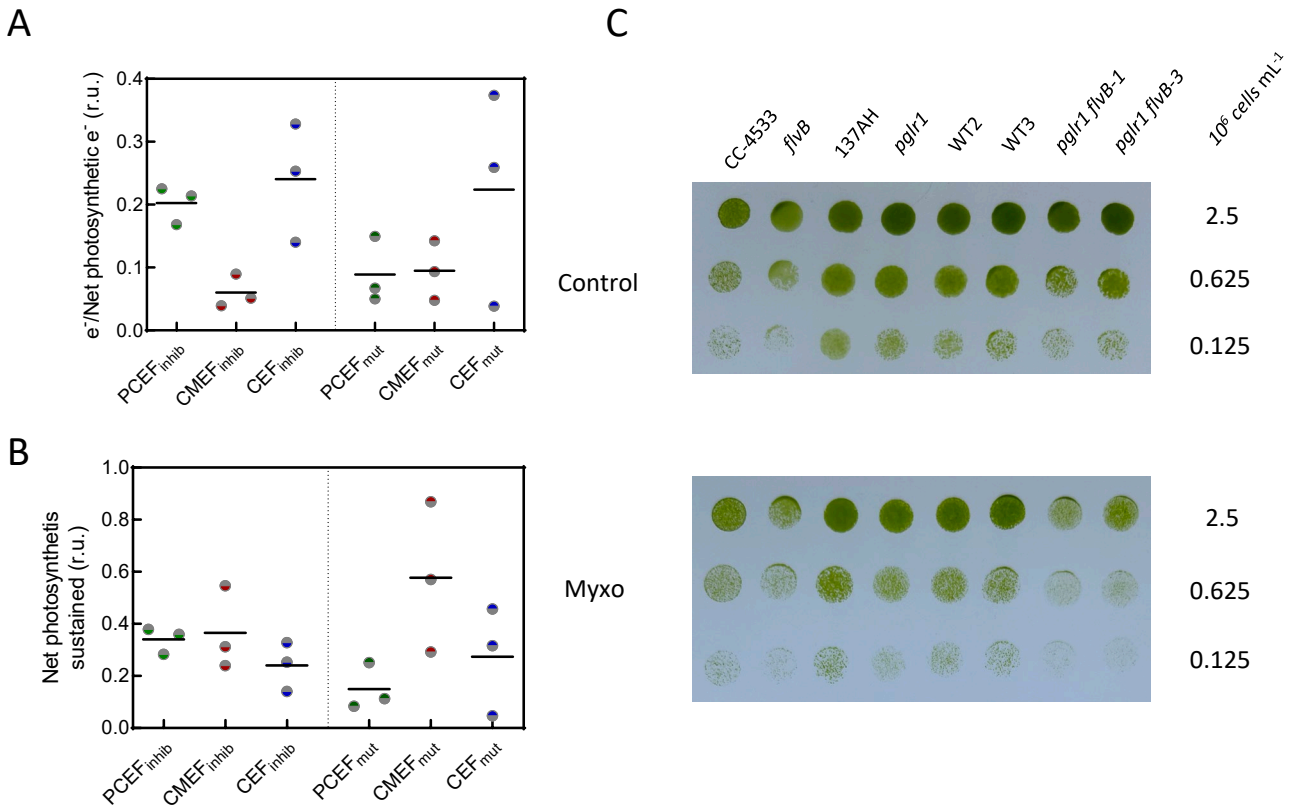

Figure 4. Contribution of CEF, PCEF and CMEF to the electron flow, net photosynthesis and growth. A Electron flow through PCEF, CEF and CMEF relative to LEF were determined in the wildtype strain CC-4533 by two different methods, one based on the use of inhibitors (inhib) the other on mutants (mut). Data used for these calculations are the same as for **Fig. 2 C** and **Sup Fig. 2**. **B** Proportion of net photosynthesis powered by each electron flow (PCEF, CEF and CMEF) in the control strain CC-4533 as measured by the inhibition (inhib) or mutant (mut) method. CC-4533 was chosen because it is the control strain for *flvB* and is therefore the only strain where both methods could be used. Data used for these calculations are the same as for **A**. In **A** and **B,** bars show the average and dots show individual replicates (*n*=3 biologically independent sample). **C**, Growth tests for *flvB* and *pgrl1* mutants, their corresponding control strains (CC-4533 and 137AH, respectively) and double mutants (*pgrl1 flvB-1 and pgrl1 flv-3*) and their corresponding control strains (WT2 and 3). Cells were spotted on plates containing minimal medium at pH 7.2 and grown under continuous illumination (60 µmol photon m^{-2} s^{-1}) in the absence (upper panel) or presence (lower panel) of 2.5µM Myxothiazol (Myxo) in air enriched at 2% CO_2. Spots shown are representative of 10 independent experiments.

Supplemental figures

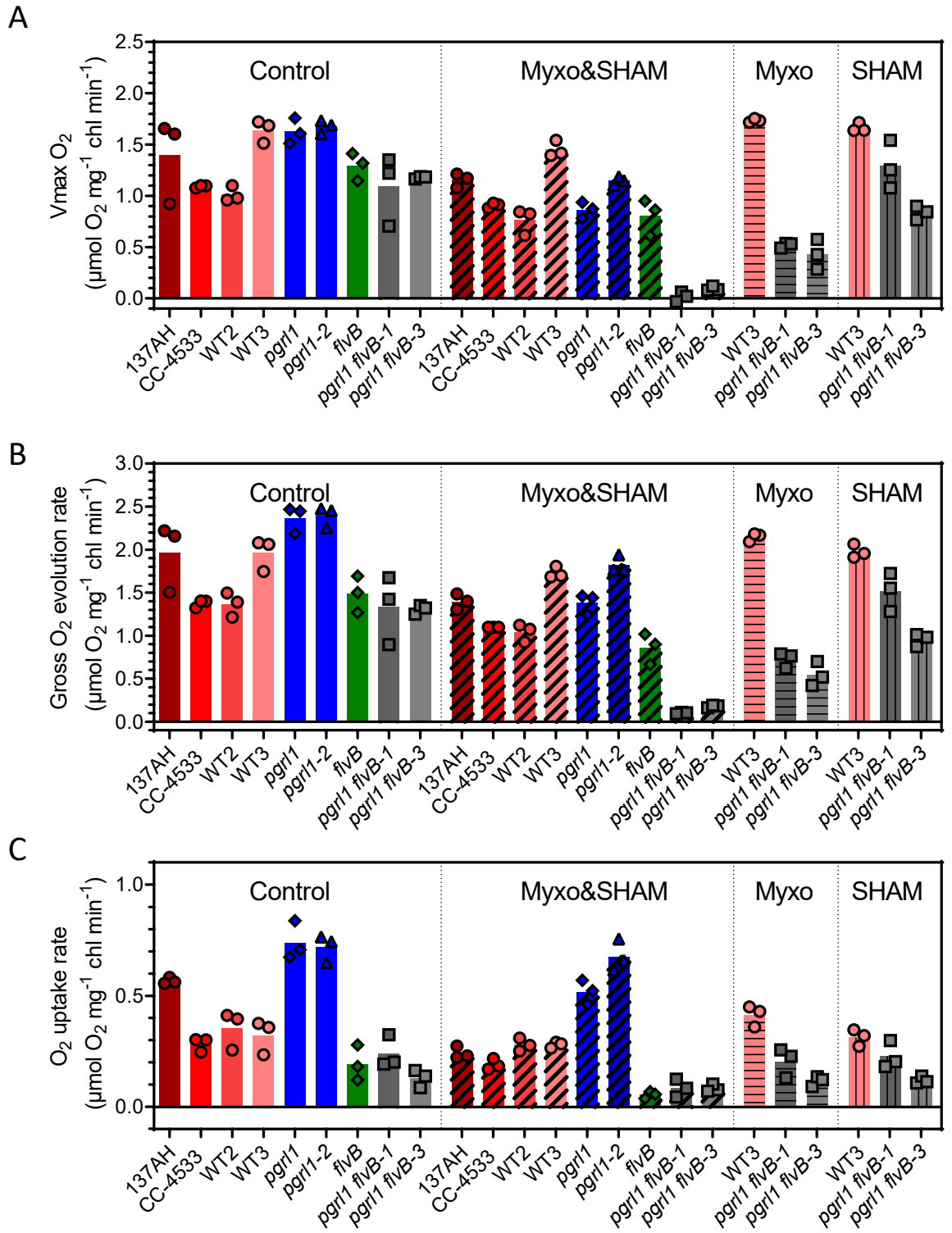

Supplemental Figure S1. Effect of mitochondrial inhibitors on O_2 exchange rates on mutants and control strains grown at air level of CO_2. O_2 exchange rates are measured from same experiments used in **Fig. 2 A-C**, **Sup Figs. S2, S3, S9, S11** and **S12**. Maximal net O_2 production (Vmax O_2) (**A**), gross O_2 evolution (**B**) and gross O_2 uptake (**C**) was measured on cells treated with myxothiazol (Myxo, 2.5 μM), salicylhydroxamic acid (SHAM, 400 μM), both Myxo and SHAM (Myxo&SHAM) or untreated (Control). Shown are the values measured after 9 minutes of illumination to reach steady state photosynthesis. Bars show the mean and dots show individual replicates (n = 3 biologically independent samples).

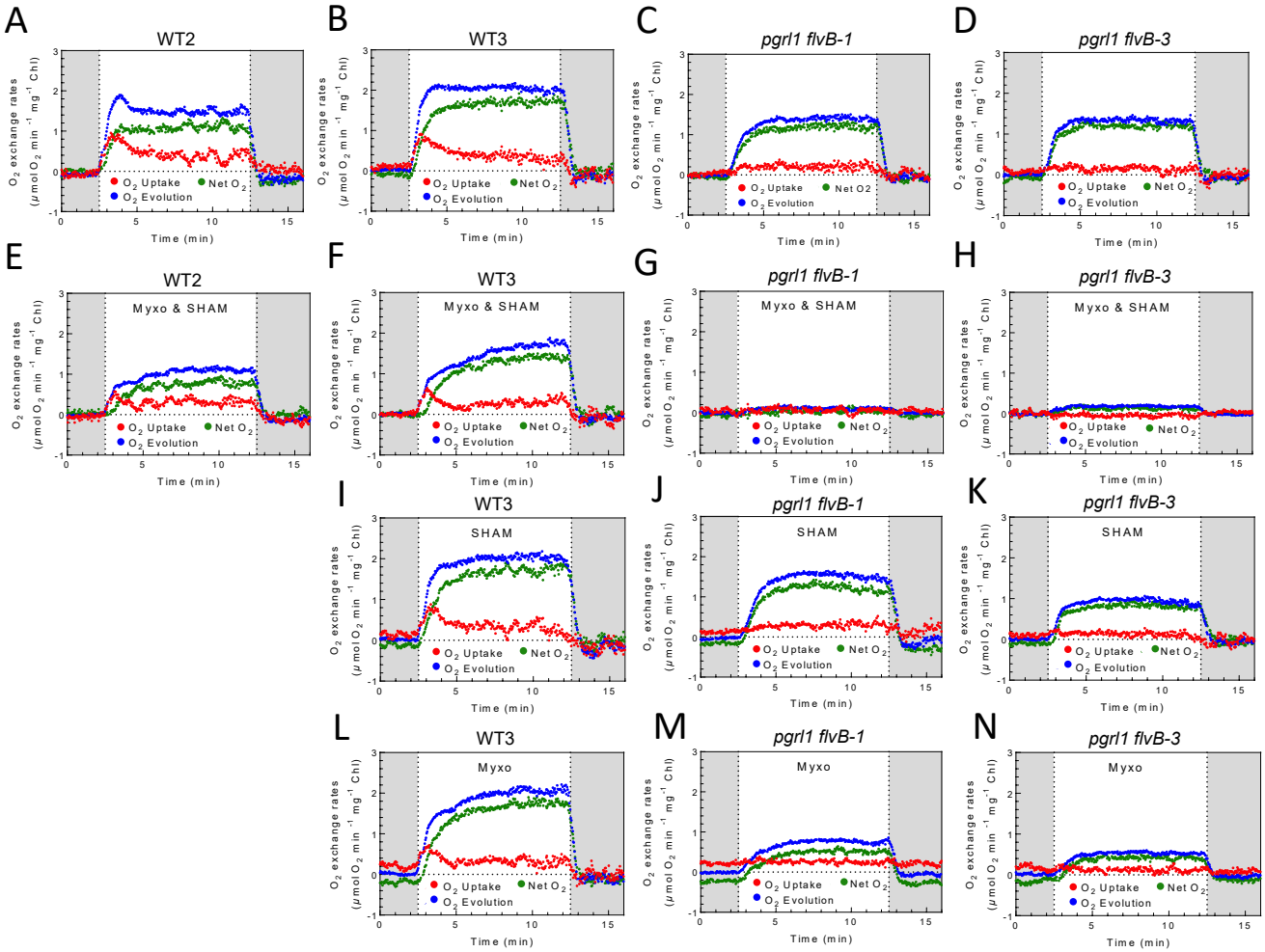

Supplemental Figure S2. O_2 exchange rated in *pgrl1 flvB* double mutants and their control strains grown at air level of CO_2. A-N Gross and net O_2 exchange rates upon a dark (grayed areas)-light-dark transition on cells treated with myxothiazol (Myxo, 2.5 μM) (**L, M, N**) , salicylhydroxamic acid (SHAM, 400 μM) (**I, J, K**) , both Myxo and SHAM (**E, F, G, H**) or untreated (**A, B, C, D**) . Cells were grown at air level of CO_2, shown are representative traces of n=3 biologically independent experiments for *pgrl1 flvB*-1 (**C, F, I, M**), *pgrl1 flvB-3* (**D, G, J, O**), *flvB* (**H, J**) and their control strains WT2 (**A, K**) and WT3 (**B, E, H, L**).

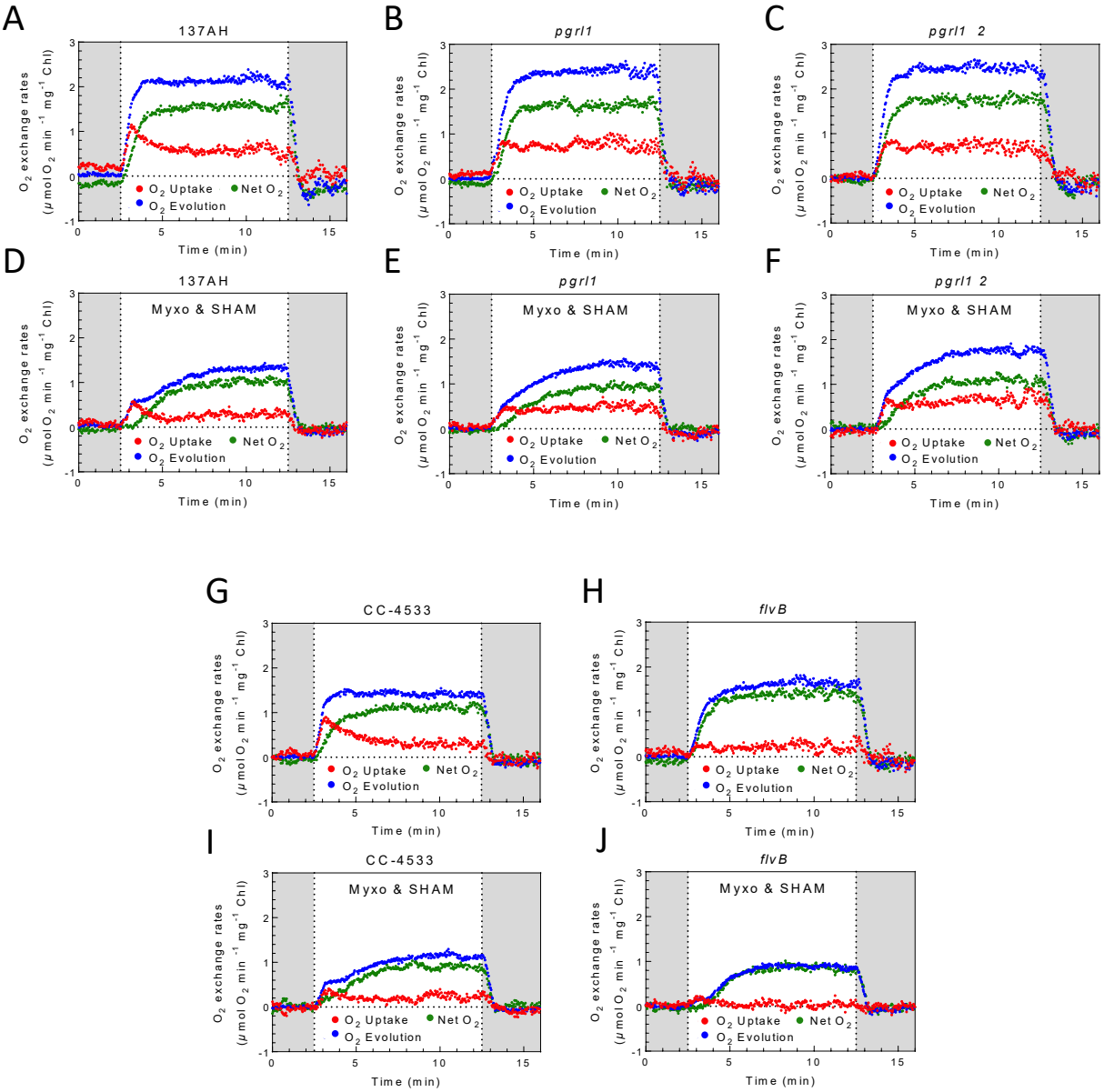

Supplemental Figure S3. O_2 exchange rated in *pgrl1* and *flvB* single mutants and their control strains grown at air level of CO_2. Gross and net O_2 exchange rates upon a dark (grayed areas) -light-dark transition on cells treated (**D**, **E**, **F**, **I**, **J**) or not (**A**, **B**, **C**, **G**, **H**) with myxothiazol (Myxo, 2.5 μM) and salicylhydroxamic acid (SHAM, 400 μM). Cells were grown at air level of CO_2, shown are representative traces of n=3 biologically independent experiments for *pgrl1* (**B**, **E**), *pgrl1* 2 (**C**, **F**), *flvB* (**H**, **J**) and their respective control strains 137AH (**A**, **D**) and CC-4533 (**G**, **I**).

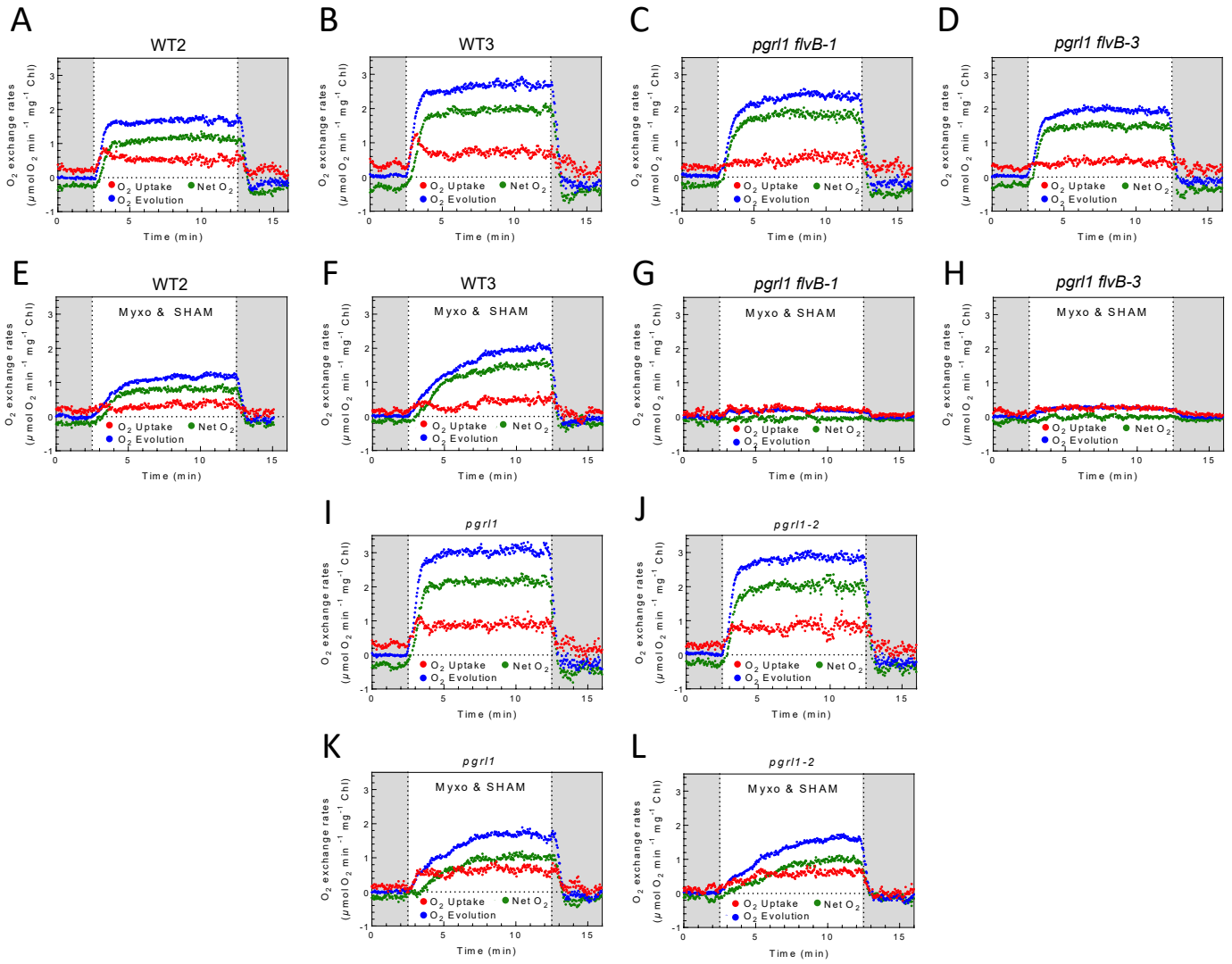

Supplemental Figure S4. O_2 exchange rated in *pgrl1, pgrl1 flvB* and their control strains grown in air enriched with 2% CO_2. Gross and net O_2 exchange rates upon a dark (grayed areas) -light-dark transition on cells treated (**E**, **F**, **G**, **H**, **K**, **L**) or not (**A**, **B**, **C**, **D**, **K**, **L**) with myxothiazol (Myxo, 2.5 μM) and salicylhydroxamic acid (SHAM, 400 μM). Cells were grown with air enriched with 2% CO_2, shown are representative traces of n=3 biologically independent experiments for *pgrl1 flvB*-1 (**C**, **G**), *pgrl1 flvB-3* (**D**, **H**), their respective control strains WT2 (**A**, **E**) and (**B**, **F**), *pgrl1* (**I**, **K**) and *pgrl1* 2 (**J**, **L**).

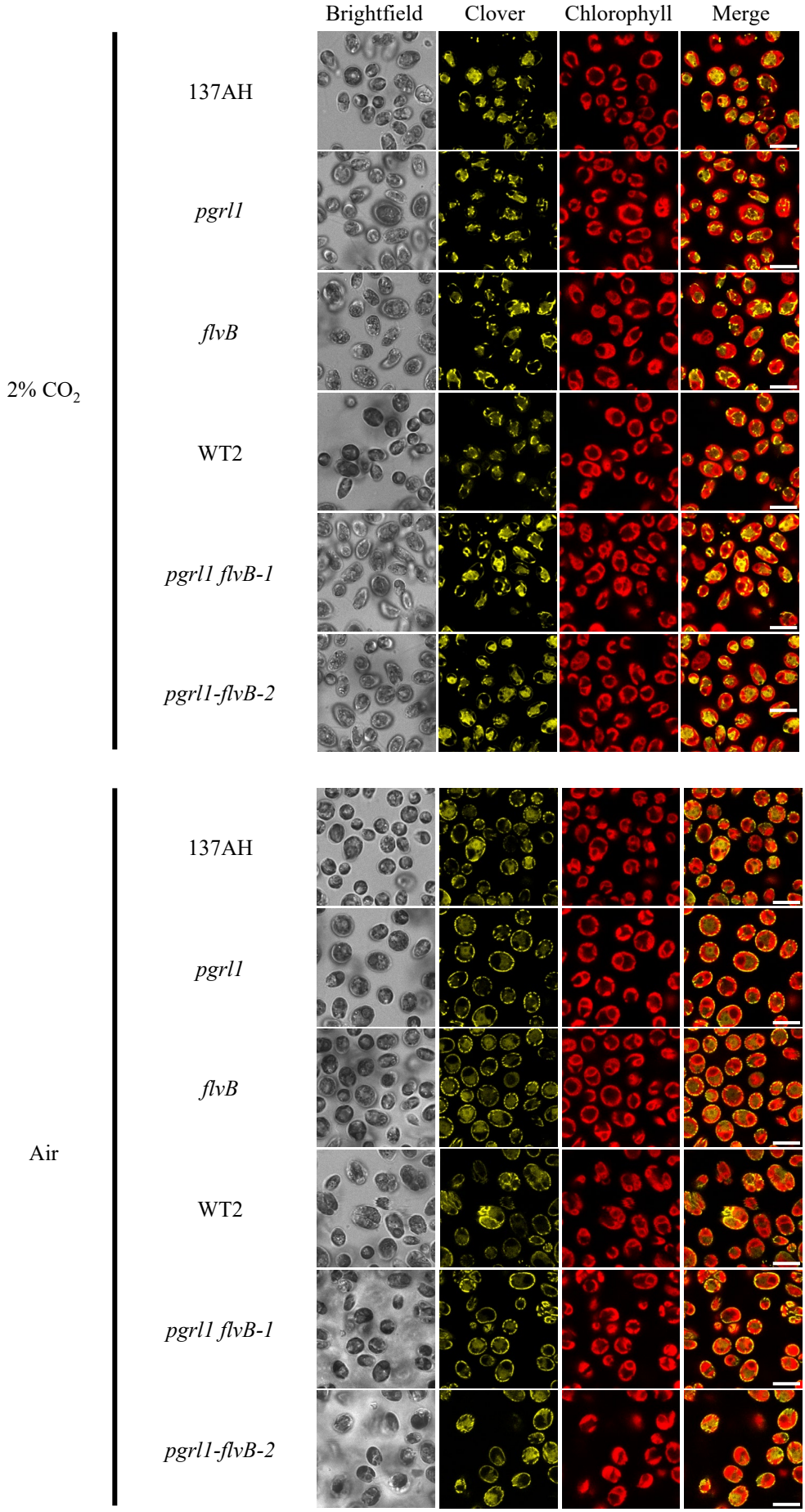

Supplemental Figure S5. Localization of mitochondria in *pgrl1*, *flvB*, *pgrl1 flvB-1* and -2 and their control strain in air enriched or not with 2% CO_2. Cross section images showing subcellular localization of the mitochondria-localized mito-Clover and chlorophyll fluorescence in *pgrl1*, *flvB*, *pgrl1 flvB-1, pgrl1 flvB-2* and the control strains 137AH and WT2, grown in air or 2% CO_2-enriched air. Shown are representative of two independent experiments.

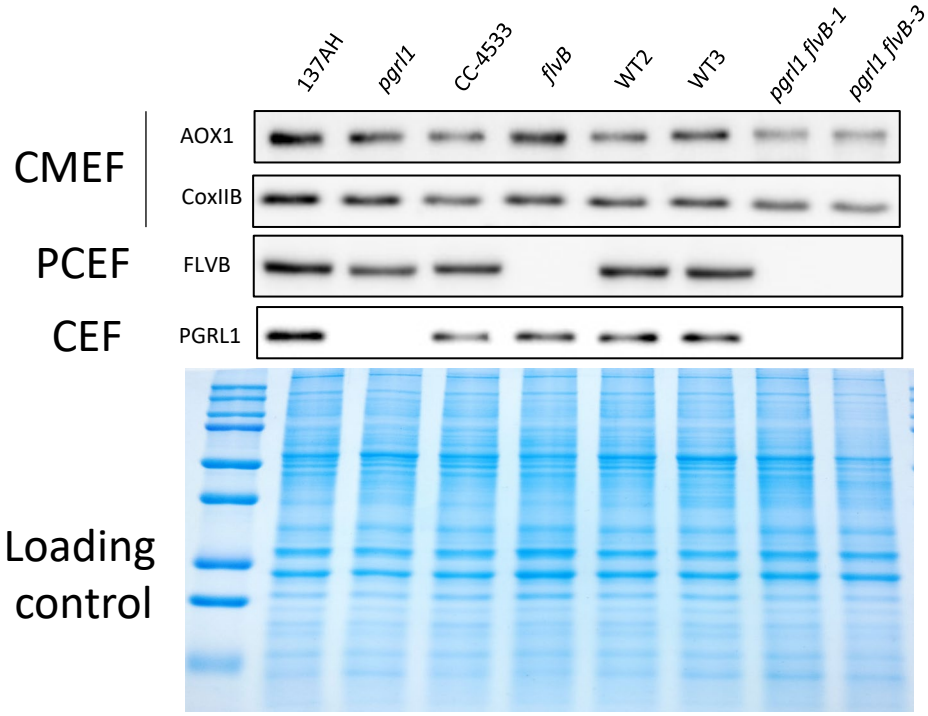

Supplemental Figure S6. Immunodetection of proteins involved in CMEF, PCEF and CEF in the strains used in this study. Immunodetection of PGRL1, FLVB, AOX1, CoxIIB in pgrl1, flvB mutants and *pgrl1 flvB* double mutants and their respective controls grown at air level of CO_2.

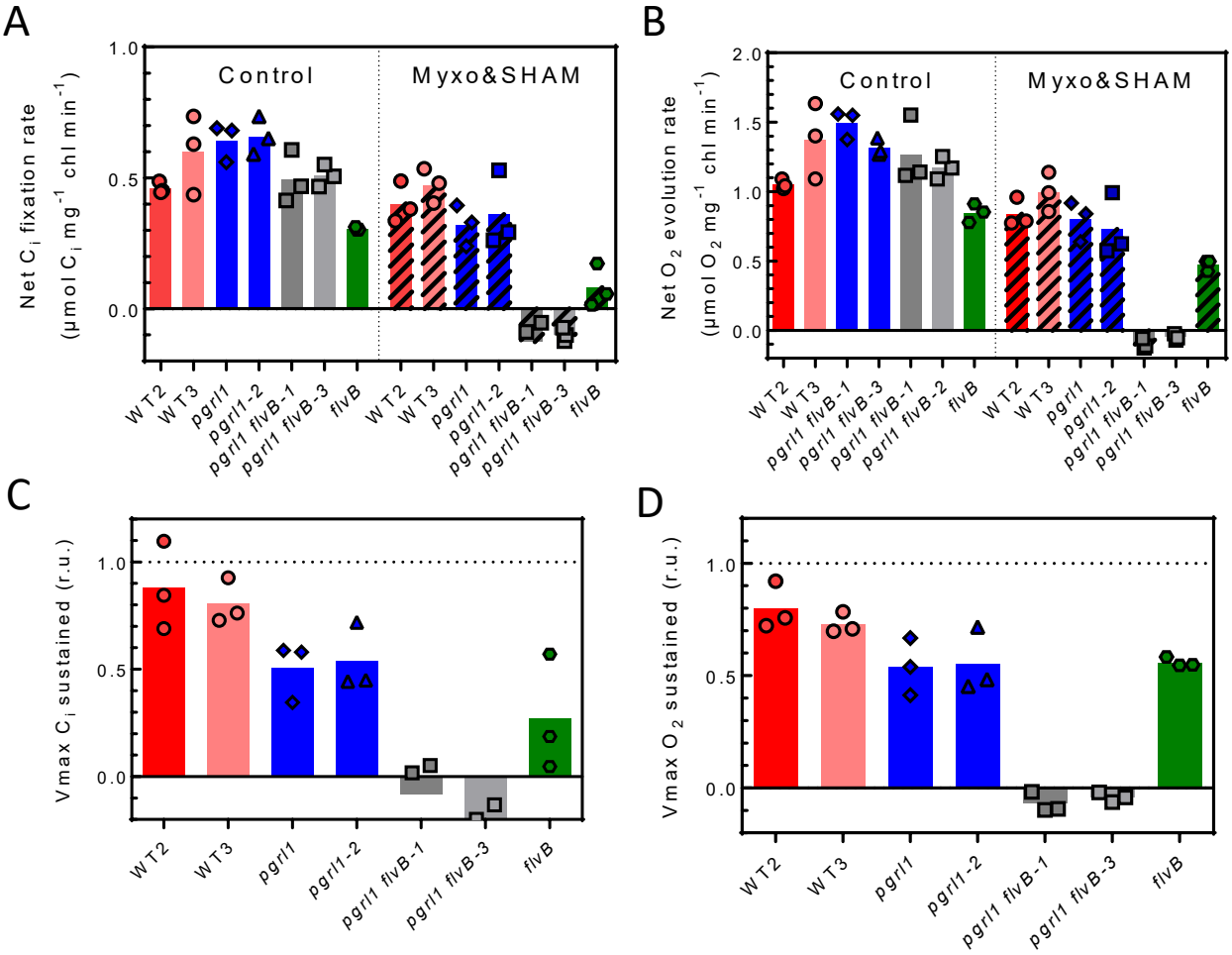

Supplemental Figure S7. Comparison of net inorganic carbon fixation and net O_2 production. Inorganic carbon (C_i) and O_2 exchange rates are measured concomitantly during a dark to light transition. Data shown are from same experiments used in **Sup Figs. S8**. **A**, **B** Net O_2 evolution (**B**) and C_i fixation (**A**) on cells treated (right panels) or not (left panels) with myxothiazol (Myxo, 2.5 μM) and salicylhydroxamic acid (SHAM, 400 μM). **C, D** Maximal net C_i fixation (**C**) and net O_2 evolution (**D**) sustained after treatment with myxothiazol and salicylhydroxamic acid. Cells were grown at air level of CO_2, shown are representative traces of n=3 biologically independent experiments for *pgrl1*, *pgrl1* 2, *flvB, pgrl1 flvB-1, pgrl1 flvB-3* and the control strains WT2 and WT3.

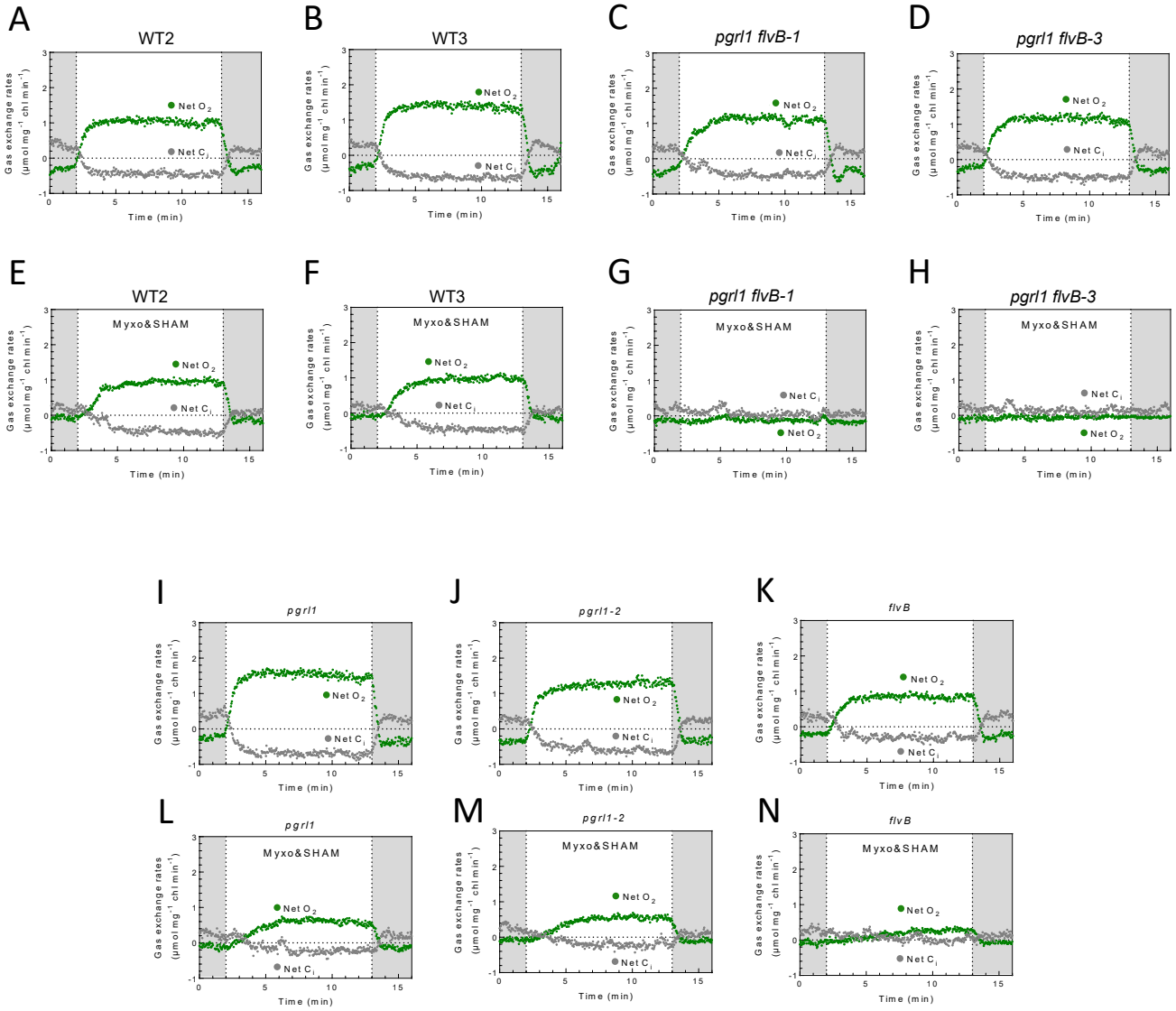

Supplemental Figure S8. Net C_i and O_2 exchange rated in *pgrl1* and *flvB* single and double mutants and the control strains WT2 and WT3. Inorganic carbon (C_i) and O_2 exchange rates are measured concomitantly upon a dark (grayed areas) -light-dark transition on cells treated (**E**, **F**, **G**, **H, L, M, N**) or not (**A**, **B**, **C**, **D**, **I**, **J**, **K**) with myxothiazol (Myxo, 2.5 μM) and salicylhydroxamic acid (SHAM, 400 μM). Cells were grown at air level of CO_2, shown are representative traces of n=3 biologically independent experiments for *pgrl1* (**I**, **L**), *pgrl1* 2 (**J**, **M**), *flvB* (**K**, **N**), *pgrl1 flvB-1* (**C**, **G**), *pgrl1 flvB-3* (**D**, **H**) and the control strains WT2 (**A**, **E**) and WT3 (**B**, **F**).

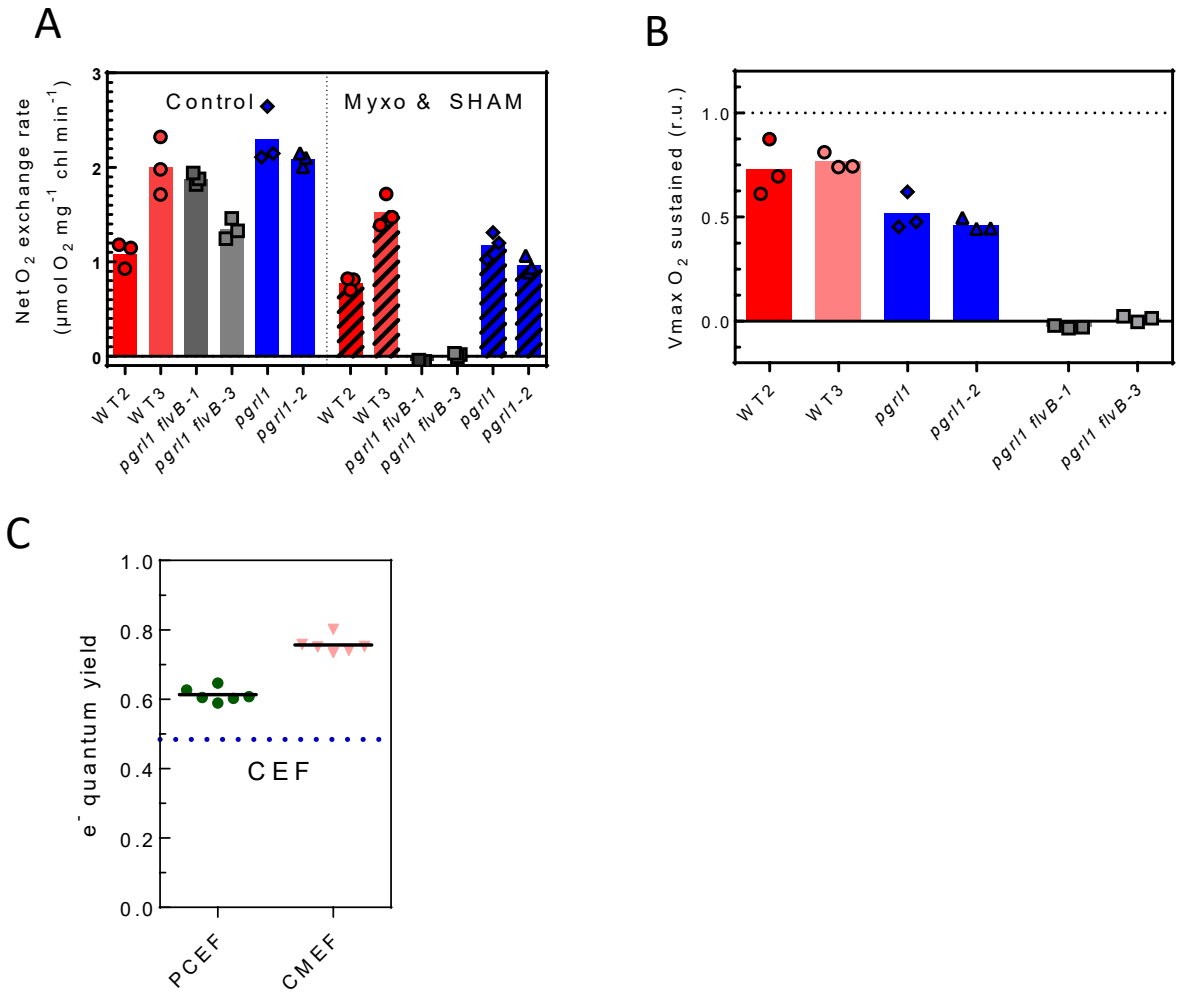

Supplemental Figure S9. Net O_2 exchange rates characteristic and e^- quantum yield measured in strains grown in air enriched with 2% CO_2. Data shown are obtained from the same experiments used in **Fig. 2 D**, **Sup Fig. S4**. **A**, Net O_2 evolution on cells treated (right panels) or not (left panels) with myxothiazol (Myxo, 2.5 μM) and salicylhydroxamic acid (SHAM, 400 μM). **B** Maximal net O_2 evolution sustained after treatment with myxothiazol and salicylhydroxamic acid. **C** Electron quantum yield of PCEF (green), CMEF (pink) and CEF (dotted line). Cells were grown in air enriched with 2% CO_2, Bars show the mean and dots show individual replicates (n = 3 biologically independent samples).

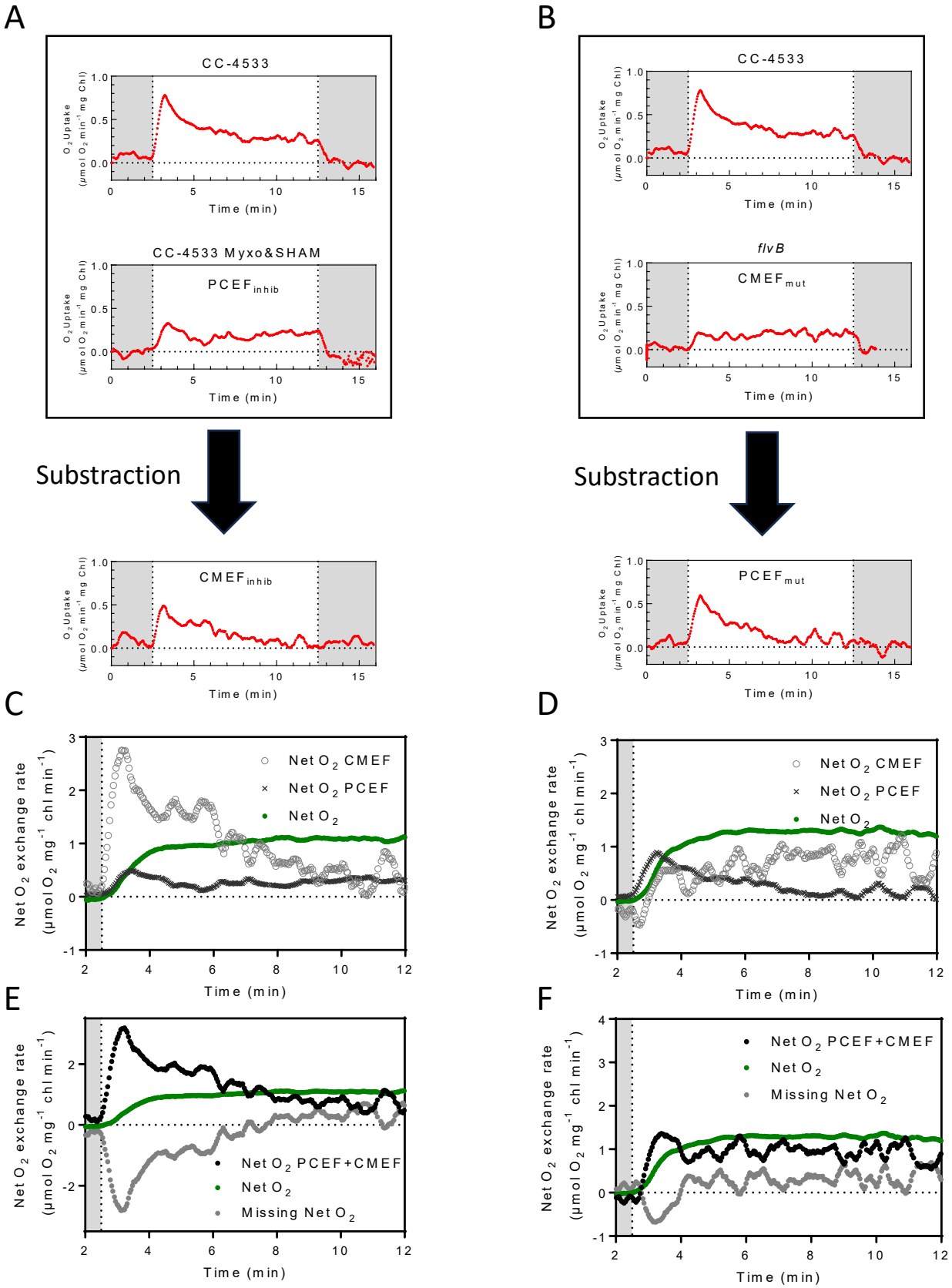

Supplemental Figure S10. Illustration of the method used to quantify of the contribution of each photosynthetic electron flow to CO_2 fixation. Illustrated here are the two different methods used, one based on the use of inhibitors (inhib) (**A**, **C**, **E**) the other on mutants (mut) (**B**, **D**, **F**). The first step for both methods is to calculate the gross O_2 uptake mediated by CMEF and PCEF either by first quantifying $PCEF_{inhib}$ and deducting $CMEF_{inhib}$ (**A**), or by first quantifying $CMEF_{mut}$ and deducting $CPEF_{mut}$ (**B**). Then, those fluxes are combined with the e^- quantum yield of each flux to predict the net O_2 evolution powered by CMEF (gray cirlces) and PCEF (gray crosses) (**C**, **D**). The net O_2 hence powered by CMEF and PCEF (gray dots) is then compared to the actual net O_2 evolution measured (green dots) to compute the net O_2 evolution that should be powered by CEF (missing Net O_2) (**E**, **F**). Shown here are average signals of n = 3 biologically independent samples.

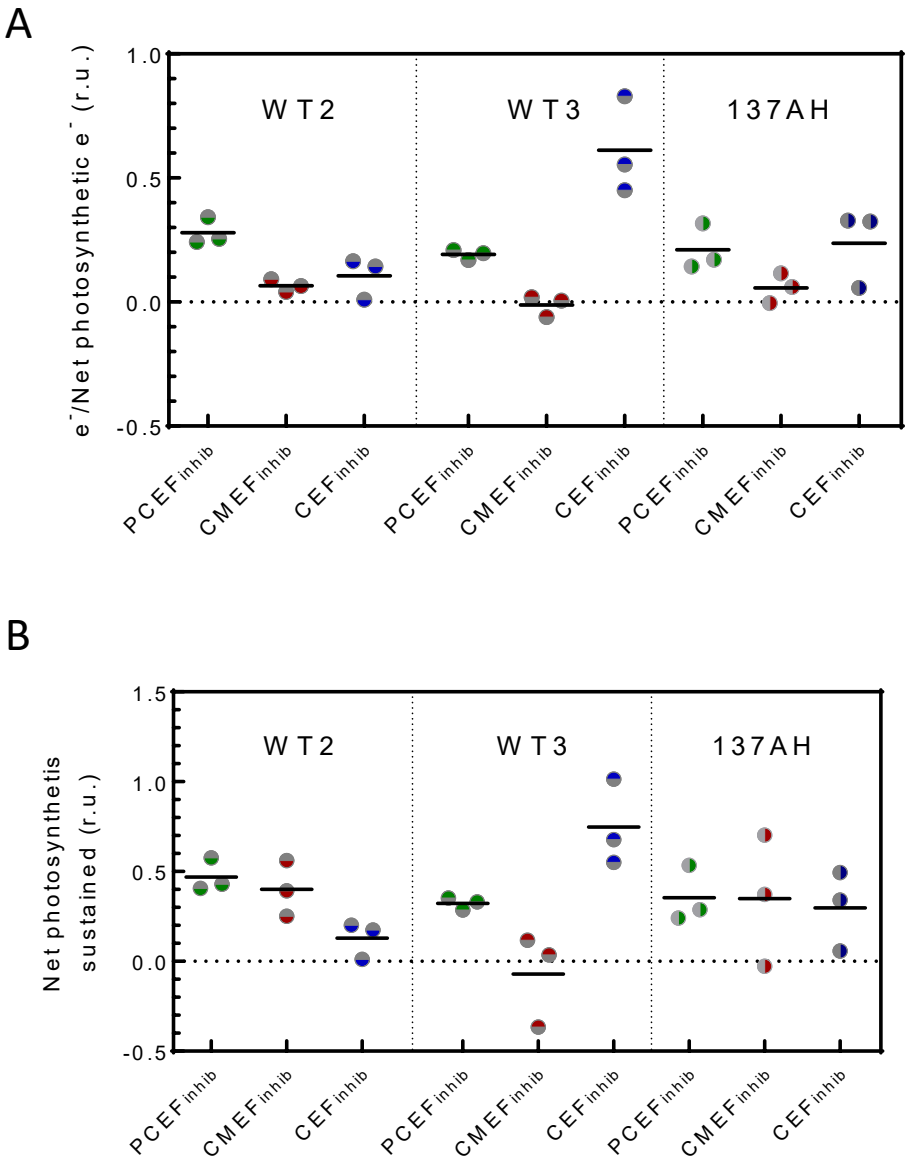

Supplementatl Figure S11. Quantification of the contribution of each photosynthetic electron flow to net photosynthesis. Data used for this calculation are the same as the one in **Supplemental Figs. S1, S2, S3.** Evaluation of the electron flow through PCEF, CMEF and CEF relative to LEF (**A**), and net photosynthesis sustained by PCEF, CMEF and CEF (**B**) based on the inhibitor method (**Sup. Fig. 12**) on WT2, WT3 and 137AH. Because of an twice greater dark O_2 uptake in 137AH, CMEF of 137AH was lowered by the dark O_2 uptake. Cells were grown at air levels of CO_2, Bars show the mean and dots show individual replicates (*n* = 3 biologically independent samples).

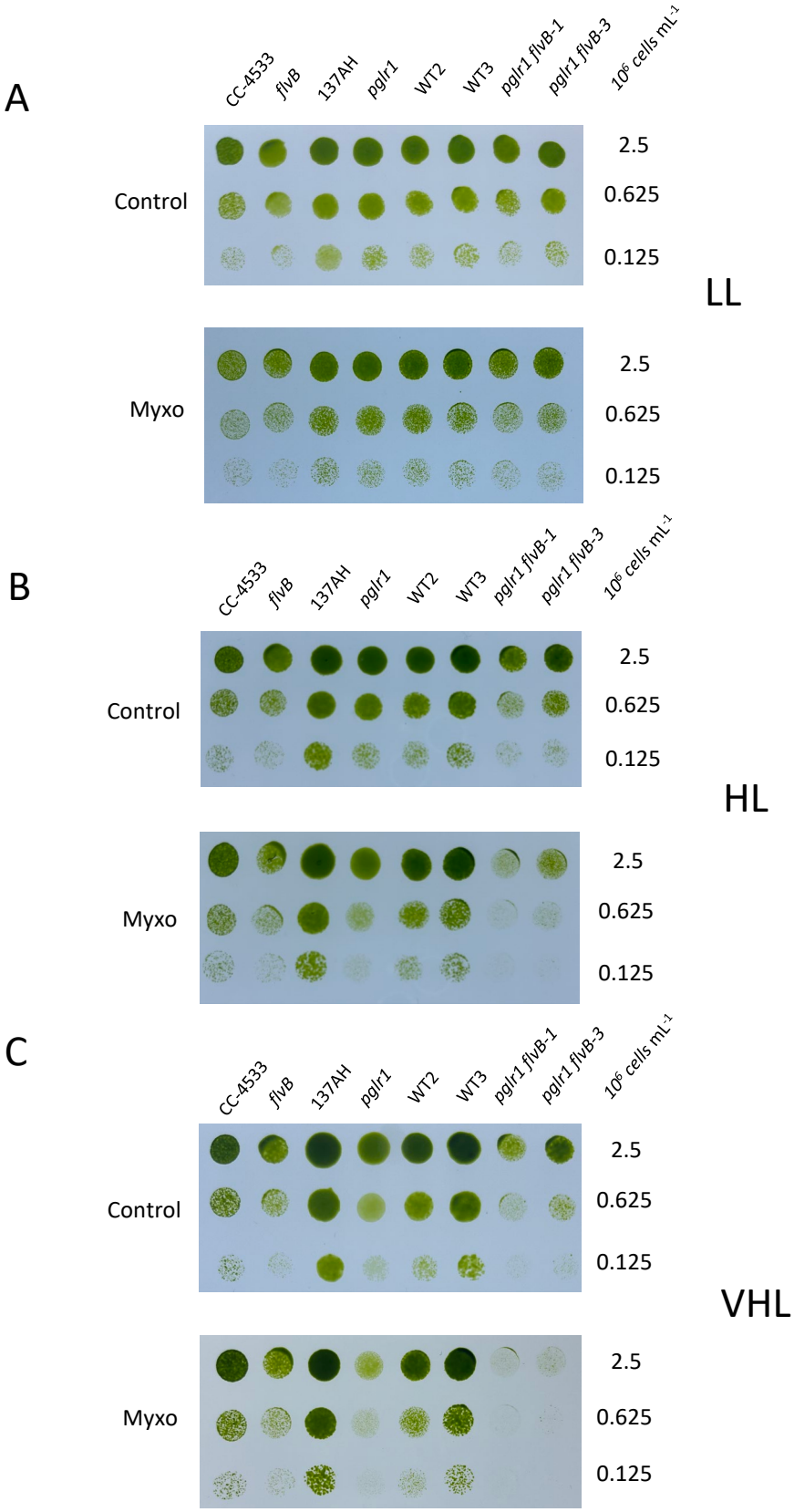

Supplemental Figure S12. Growth of mutant and control strains at various light intensities. Cells were spotted on plates containing minimal medium in the absence (control) or presence (Myxo) of myxothiazol (2.5µM) and grown under low light (LL, 30 µmol photons m^{-2} s^{-1}), high light (HL, 100 µmol photons m^{-2} s^{-1}) or very high light (VHL, 200 µmol photons m^{-2} s^{-1}). Cells were grown in air enriched with 2% of CO_2 at 25°C. Growth was assessed after three days in *pgrl1*, *flvB*, and their respective control strains (137AH and CC-4533) and on double mutants (*pgrl1 flvB*-1 -3) and their control strains (WT2, WT3). Shown are representative spot tests of n = 10 independent experiments.

Source Data

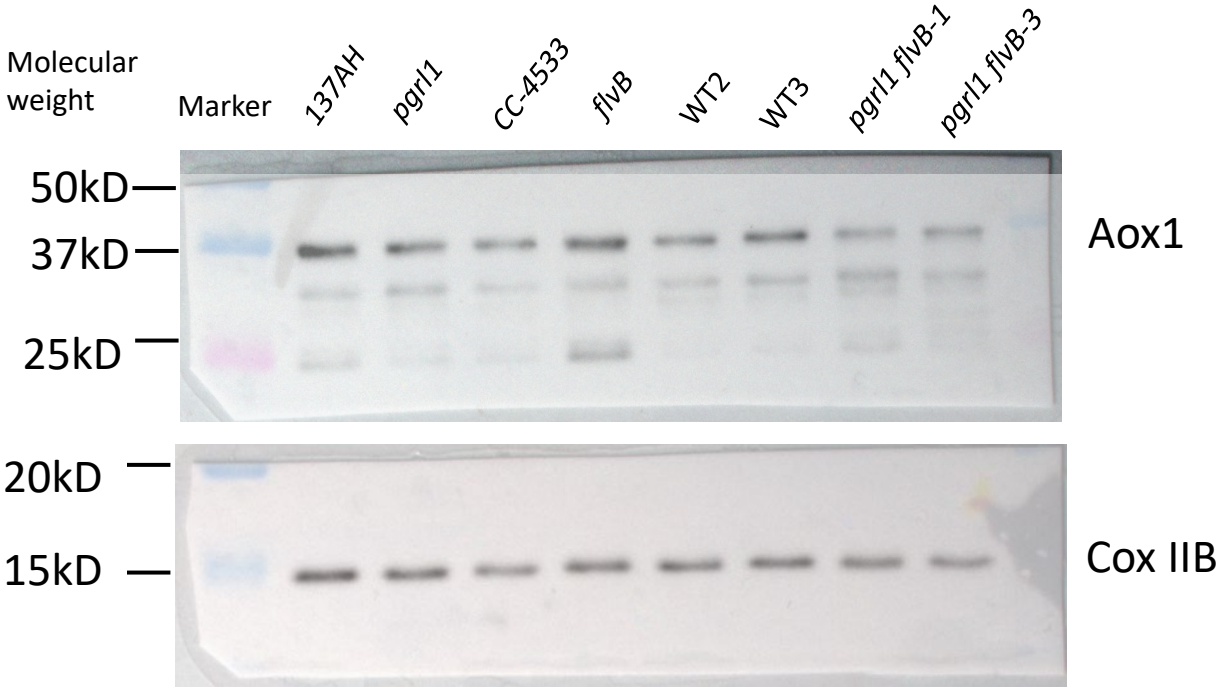
Molecular weight
Marker
137AH
pgrl1
CC-4533
flvB
WT2
WT3
pgrl1 flvB-1
pgrl1 flvB-3
50kD
37kD
25kD
Aox1
20kD
15kD
Cox IIB

Aox 1

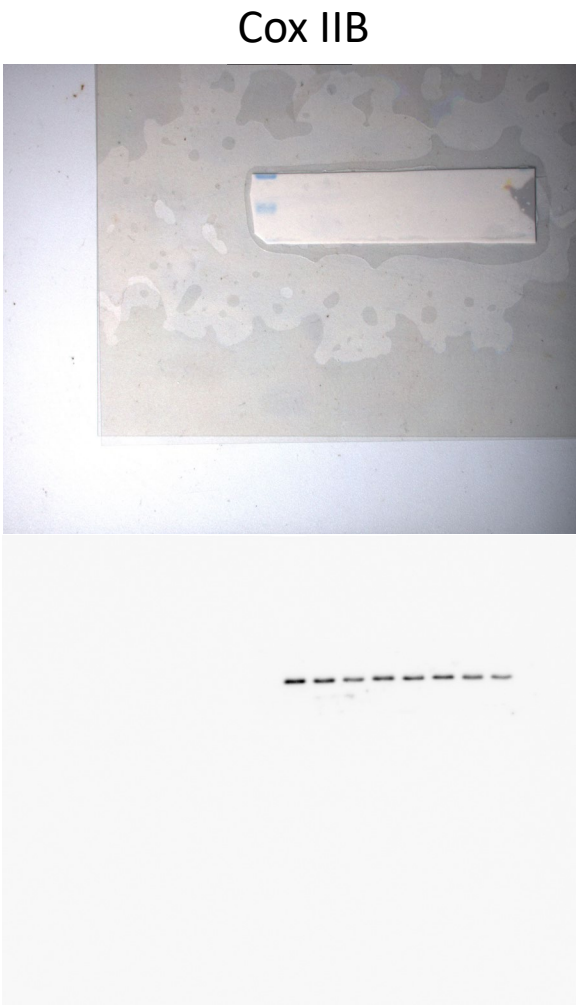
Cox IIB

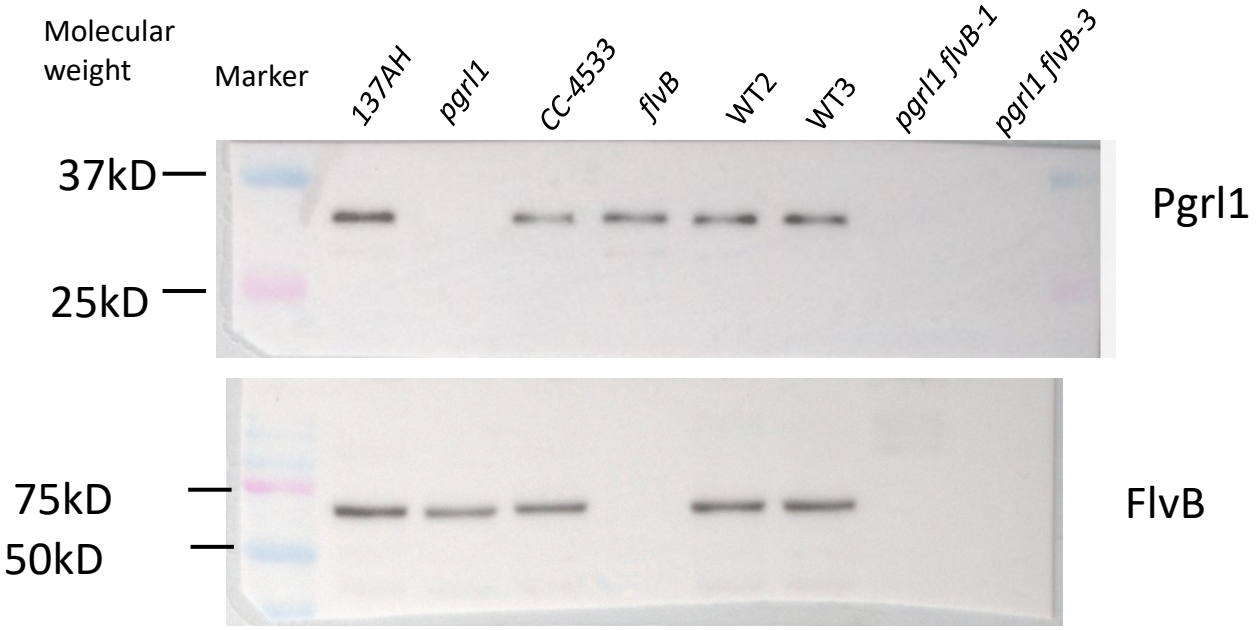
Molecular weight
Marker
137AH
pgrl1
CC-4533
flvB
WT2
WT3
pgrl1 flvB-1
pgrl1 flvB-3
37kD
25kD
Pgrl1
75kD
50kD
FlvB

FlvB
Pgrl1